FINAL REPORT:

1606 ATP / RD390

Autoignition Fuel Spray Injector Development

Aimee Williams, Eugene Lubarsky, Svyatoslav Yorish, and Ben T. Zinn

Georgia Institute of Technology
Atlanta, GA

March 14, 2013

Abstract

This study characterizes the performance of two solid-cone spray nozzles in order to determine the uniformity of each nozzle with the intention of using the nozzles for fututе autoignition testing. These nozzles were embedded in a bullet-shaped body supported by three hollow pylons. The three pylons allow for cooling air and one includes a 1/16" stainless steel tube for fuel supply or nitrogen purge of the injector. The nozzles were placed in a flow reactor designed to simulate conditions in a jet engine thrust augmentor. In this facility, preheated air at an average of 650°C, 125 m/s, 11.8% O_2 was in co-flow with the injector and the 45mm (1.77") I.D. quartz silica test section allows for full optical access. This design provides minimal flow disturbance . Both nozzles appeared to be solid cone by visual inspection. Droplet sizes and velocities were measured using a TSI three component Phase Doppler Particle Analyzer (PDPA). With the supplied software, Sauter and arithmetic mean diameters were calculated at 4 cross sections in the flow (Z = 10, 20, 30, and 40 mm from the nozzle exit). For both nozzles, large droplets were deposited near the periphery of the spray. The HAGO nozzle produced average droplet sizes of 15μm SMD in the center of the spray and a maximum average droplet of 70-80μm SMD near the edge. The BETE nozzle produced smaller droplets, with 10μm SMD in the center and 35-70μm near the edge. The BETE nozzle produced a much wider spray angle and at 40mm the spray filled the entire cross-sectional area of the test section. Additionally, the BETE nozzle produced a much faster spray, with velocities around 90 m/s at 40mm from the nozzle, with the HAGO nozzle only at 60 m/s in an 125 m/s co-flow. Data rate shows that the center of the BETE spray is void of droplets until approximately 40% of the maximum spray radius in each cross-section. The BETE nozzle did not produce a solid-cone spray. Of the two nozzles, the HAGO nozzle produced a more uniform droplet and velocity distribution.

Introduction

Auto-ignition is the process by which a combustible mixture eventually ignites due to a build-up of chemical reaction rates, without an external ignition source. Processes such as scramjets, pulsed detonation engines, and diesel engines employ auto-ignition, while many other systems, especially gas turbines, avoid it due to the physical damage and unpredicted changes in performance that can occur when auto-ignition happens in unexpected regions. The time from injection to ignition, known as ignition delay, is a key parameter to determining the engine design. With liquid, non-premixed fuels, the time between fuel injection and ignition can consist of a physical delay of spray formation, evaporation, and mixing and a chemical delay during which the chemical reaction between the fuel and oxidizer raises the temperature and the reaction rate until ignition occurs [1, 2]. In addition to the challenges presented by a liquid fuel, the fluid mechanics, such as fluid-dynamic strain-rate, mixing, and turbulence intensity [3], of the flow reactor can affect auto-ignition.

A typical auto-ignition experiment consists of preheated air in a flow reactor, either by electric heater or combustion, and fuel injection into a test section. Fuel injection has been done either by prevaporized or liquid fuel injection. Methods of determining auto-ignition have varied from human inspection of ignition location, chemiluminescence imaging, and temperature measurements. Alternatively, auto-ignition can be investigated in shock tubes, rapid-compression machines, and constant volume combustors, although these measure ignition delay times of prevaporized kerosene type fuels when the influence of fluid mechanics and droplets was not wanted [4].

Several studies have calculated the auto-ignition delay of kerosene-air mixtures in continuous flow combustors in the past 70 years. These experiments generally use pre-vaporized kerosene (4 to 8) or liquid fuel injectors that disturb the flow [2, 10, 11]. Computational studies, such as Mastorakos found that auto-ignition preferentially occurs at the most reactive mixture fraction[12], while Kreutz and Law [13] found that kernels occur at the location of maximum temperature.

Auto-ignition is generally described using the Arrhenius rate equation shown below. In this equation, A represents a pre-exponential factor, which depends on statistical mechanics and collision theory, E_a is the activation energy of the fuel, R is the universal gas constant, and T is the temperature of interest. These values are generally found experimentally when measured ignition delay time versus temperature is plotted on a log-linear plot. The slope of the resulting line is $\frac{E_a}{R}$. For Jet-A, and other similar kerosene-type fuels, the activation energy has been experimentally determined to be approximately 40 $\frac{kcal}{mol}$.

$$t_{ign} = A \exp(\frac{E_a}{RT}) \tag{1}$$

In addition to prediction models, Auto-ignition is used to validate chemistry mechanisms and surrogate fuel models for complicated fuel mixtures, such as Jet-A [14]. Shock tube and rapid compression machine techniques are generally used for this, but they do not capture the influence of fluid mechanics on ignition delay times.

With the high turbine exit temperatures of current and future gas turbine engines, the fuel injected in reheat combustors is at sufficiently high temperatures to auto-ignite within the confines of the reheat area. Unwanted auto-ignition provides a limitation on the design of current reheat combustors, but if a constantly auto-igniting flame could be used in place of a bluff-body stabilized flame the pressure drop and materials limitations would be lessened or eliminated. According to Ref. [15], turbine exit temperatures can exceed 1300K which results in a maximum premixing distance of 50mm before autoignition occurs.

For a constantly auto-igniting flame to be a feasible solution in a reheat combustor, the resulting flame must be stable, compact, and reliable over a wide range of operating conditions. The idea of an auto-igniting afterburner flame with the assistance of highly reactive partially oxidized fuel injection as a pilot or flame

stabilization method has been previously investigated at Georgia Tech [16]. Additionally, injecting fuel upstream of a turbine to allow for sufficient pre-heat time has also been investigated [17, 18].

The current study investigated the performance of an aerodynamic liquid fuel injector, utilizing a solid-cone injector embedded in a bullet-shaped body supported by 3 struts, designed to minimize flow disruption and distribute fuel throughout the entire test section, with the potential of measuring auto-ignition of liquid Jet-A injected into high temperature and velocity co-flow. This injector represents a best-case scenario for fuel injection because it minimizes the time scales related to jet breakup and droplet formation if the fuel was injected as a liquid jet. This study is the first step in developing a reliable auto-ignition experiment.

Experimental Facility

High Velocity Ignition Facility

The experimental facility used for this study was designed to simulate flow conditions in a jet engine thrust augmentor. A schematic of the high velocity ignition facility (HVIF) is shown in Figure 1. This facility consisted of a stagnation point reverse flow (SPRF) combustor vitiator, dilution section, flow conditioning measuring section, liquid fuel injection section and transparent test section.

A SPRF combustor was used in this rig due to potentially high combustion efficiency and minimum disturbances it may apply to the flow. Cold air was supplied to the SPRF combustor at the base of the SPRF, which then passed along the outside of the combustor can for cooling the combustor liner and pre-heating the air flow. Natural gas and now pre-heated air were injected radially inward in distributed jets. The mixture is then impeded by a cylindrical insert and forced down to the base of the combustor can where a stagnation point was formed. A spark igniter with hydrogen purge was located at the base of the vitiator. Cold, diluting air was introduced in the form of cross-flow jets just downstream of the vitiator to allow for control of the temperature and oxygen content.

Air was supplied to vitiator and dilution section from the 125 psig laboratory air tanks and regulated to 40 psig. Total air flow rate was measured using an orifice plate equipped with upstream static pressure and differential pressure sensors and controlled by a manual gate valve. Diluting air was withdrawn from the total air flow rate and controlled via a manual gate valve. Natural gas was supplied to vitiator from the city line at 32 psig and was also metered using an orifice plate and pressure transducer system and was controlled by a manual needle valve.

The flow conditioning measurement section was a 2 inches diam. (I.D.=53 mm), 30 cm long stainless steel pipe with entrance end connected to a flange through which dilution air jets were injected. The other end of this pipe was connected to the fuel injection flange. The pipe was externally cooled using a system of air jets supplied from the shop air supply line. This pipe contains a Bosch LSU42 O2 sensor with Innovate Motorsports 3769 LC-1 Wideband Controller Lambda Cable and a Omega K-type un-grounded thermocouple. Measuring devices were installed approximately four inches upstream of the point of fuel injection with minimized intrusion into the flow.

The liquid fuel injection section of the rig provided smooth transition from the I.D.=53 mm inches of the conditioning measuring section to the transparent test section I.D= 45mm inches. Overall cone angle was 11° (5.5° on each side). Fuel was injected from an aerodynamic bullet-shaped body, with maximum diameter of 7mm, centered in the flow using 3 airfoil-shaped pylons. A picture of this fuel injection body is shown in the bottom right hand corner of Figure 1. In this image, the pylons are being held to the center body for welding using a specially designed clamp to hold the parts in alignment. The pylons are hollow to allow for cooling air to pass through. Jet fuel was supplied through a 1/16 inch (1.6 mm) stainless

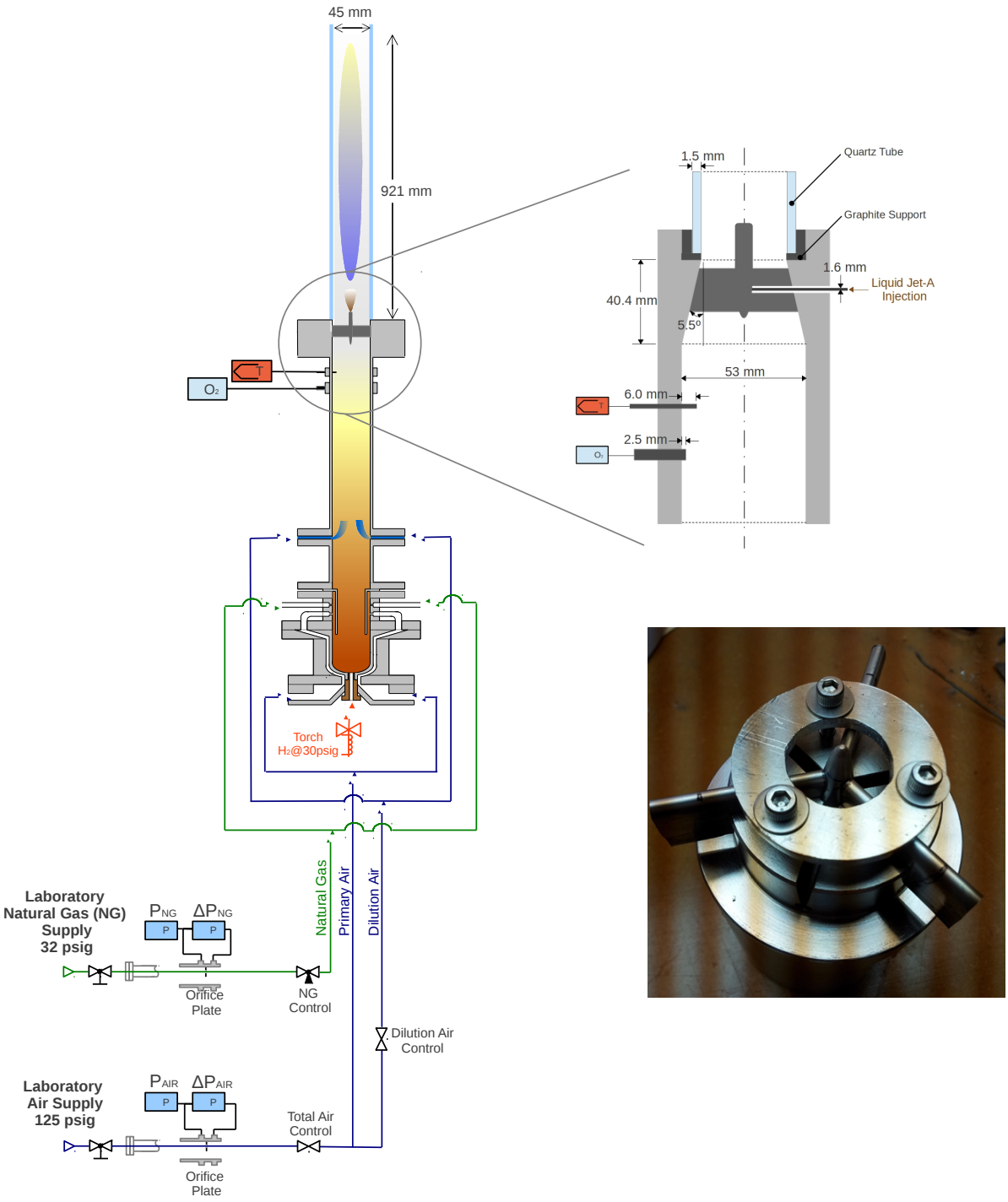

Figure 1: Schematic of HVIF with detailed view of injection section

steel tube through one of the pylons. Two commercially available nozzles, a HAGO and a BETE nozzle, were reshaped to be more aerodynamic (by grinding off hex ends and threading) and each was welded to the end of the bullet for testing. The details and performance of each nozzle is shown in the next sub-section.

The test section consisted of a quartz silica transparent tube I.D.=45 mm and 0.92 m long with the lower end set upon the shoulder of the injection section and the other end supported by a clamp attached to the structure of the rig.

Flow velocity in the test section was calculated from the total air and natural gas flow rates, taking into consideration the density change due to vitiation. The calculation of a global Jet-A, vitiated-air mixture equivalence ratio was based upon the air and natural gas flow rates and a new stoichiometry calculated from the oxygen content of the vitiated flow. Equations 2-5 outline the procedure for calculating global Jet-A, vitiated-air mixture equivalence ratio. The constants in Equation 3 are determined from equilibrium calculations of natural gas - air reactions at a range of equivalence ratios. Equation 4 calculates a new stoichiometry for the Jet-A and vitiated air reaction based on the reduced oxygen levels.

$$\phi_{vit} = \frac{\dot{m}_{NG}}{\dot{m}_{air}} * 17.12 \tag{2}$$

$$O_2(\%) = 0.0223\phi_{vit}^2 - 0.231\phi_{vit} + 0.2094 \tag{3}$$

$$\bar{S} = \frac{0.2095}{O_2\%} * 14.2467 + 0.42281 \tag{4}$$

$$\phi_{JetA} = \frac{\dot{m}_{JetA}}{\dot{m}_{air} + \dot{m}_{NG}} * \bar{S} \tag{5}$$

Liquid Jet-A fuel was supplied from a one gallon double ended Swagelok DOT-3A1800 stainless steel high pressure cylinder shown in Figure 2. This cylinder was pressurized from the top end with 50 psig nitrogen. The bottom end of the cylinder was used for supply and refueling. When supplying, fuel flows through an Arrow, 25 micron, in-line filter before metering in an <Omega> type 9401 turbine flow meter connected to FLSC-AMP <Omega> preamplifier and DP-F31-LIN <Omega> display with linear corrector and analog output to the computer. A needle valve was used to control Jet-A flow rate and a 3-way valve switched the system from Jet-A flow to a nitrogen purge, which prevented injectors from clogging during gaps in the injection sequence.

Fuel Injector Nozzles

Two commercially available nozzles were characterized for this study. They are referred to by their brand names HAGO and BETE. Each nozzle was cut in half in order to view the inner workings and the section views of both nozzle are shown in Figures 3a and 3b. In the HAGO nozzle, fuel enters into a cavity, is forced around a spring, then enters radially into a conical cavity before it is injected into the flow through a small cavity. In the BETE nozzle, fuel passes around a center body and enters into a circular cavity tangentially at the walls and is then injected into the flow via a converging nozzle. Note that the filter shown in the HAGO section view was not used as an in-line fuel filter is already installed.

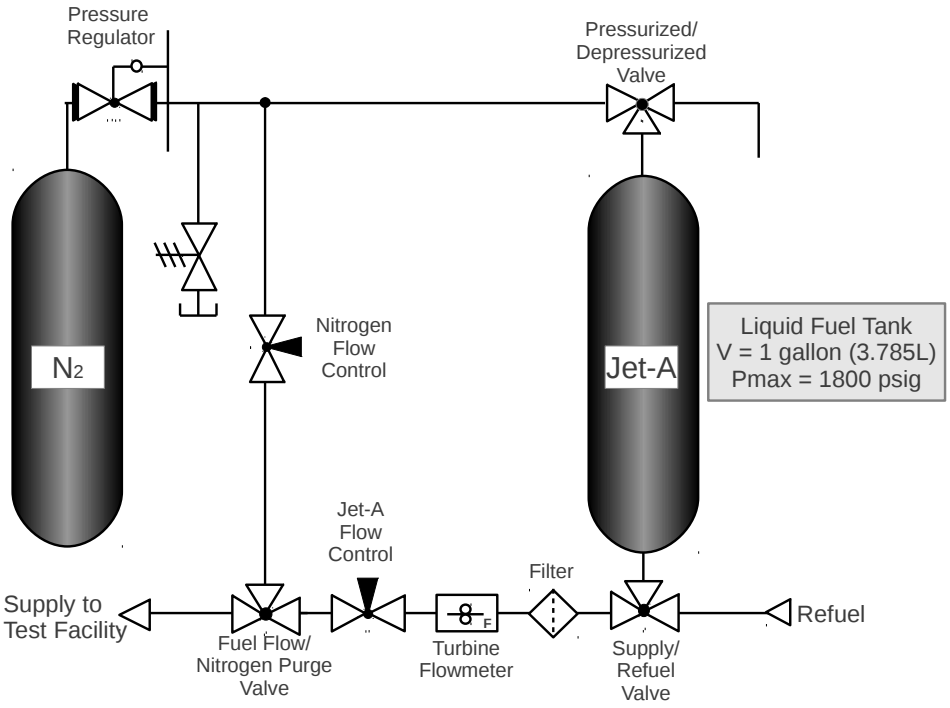

Figure 2: Schematic of Jet-A supply system

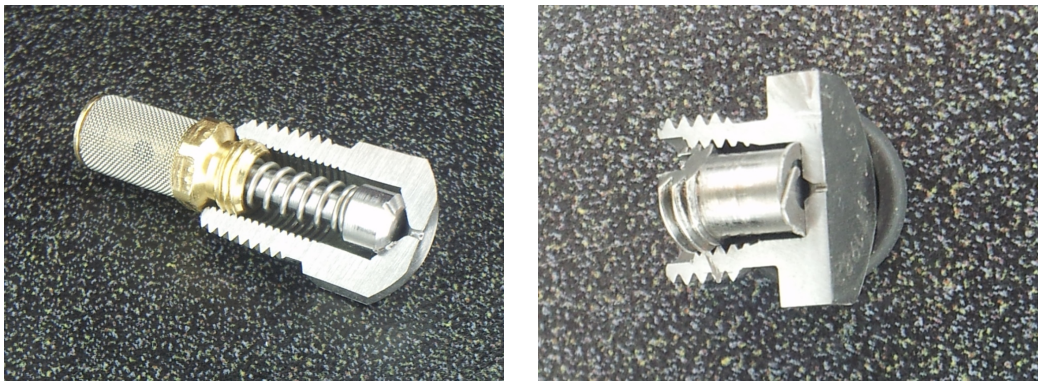

(a) HAGO (b) BETE

Figure 3: Section view of spray nozzles

Methodology

During this study, two nozzles underwent hydraulic testing and spray angle observation, without co-flow, then were installed in the high velocity ignition facility in the co-flow of hot, vitiated air and droplet size and velocity measurements were obtained.

Test Procedure for Droplet Size and Velocity Measurements

During a typical experiment, flow conditions were set to a desired temperature of 650°C, velocity of 125 m/s, and oxygen content near 12% using the air and natural gas flow rate and dilution air controls. Once the flow reached a steady temperature, Jet-A was injected at the desired flow rate (0.8, 1.6, 2.4 g/s). At each mass flow rate, droplet size and velocity measurements were collected in a grid pattern in four planes (Z = 10mm, 20mm, 30mm, and 40mm) using a TSI three component Phase Doppler Particle Analyzer (PDPA). A top-down schematic of the system orientation with respect to the injector is shown in Figure 4b and the coordinate system used in this study is illustrated below in both Figures 4a and 4b. The X,Y, and Z axes are defined by the motion of the traverse and the 2-component PDPA transmitter, which measures V_x, V_z, and droplet size, is aligned with the Y-axis in the -Y direction, while the single PDPA transmitter measuring V_y is aligned with the X axis in the -X direction.

Figure 5 shows the traverse matrices used in these experiments. At each location, measurements were collected for 10 seconds or until a maximum of 10,000 droplet measurements was reached. Table 1 shows a summary of all test conditions at which these measurements were obtained.

Table 1: Summary of test conditions

Vel (m/s)	T ($^{\circ}C$)	$O_2(\%)$	$\dot{m}_{JetA}(g/s)$	Z (mm)	P $_{JetA}$ (psia)	Nozzle
123.6	647.2	11.5	0.75	10	25.5	HAGO
117.7	647.4	11.6	1.62	10	54.3	HAGO
122.9	646.7	11.6	2.39	10	91.9	HAGO
123.4	650.4	11.8	0.76	20	26.3	HAGO
123.2	646.2	11.9	1.60	20	54.0	HAGO
122.7	648.4	11.9	2.41	20	92.5	HAGO
125.3	646.4	12.0	0.79	30	26.3	HAGO
126.5	658.2	11.7	1.59	30	11.1	HAGO
126.4	656.3	11.7	2.40	30	11.1	HAGO
122.0	650.4	11.9	0.76	40	25.9	HAGO
121.7	650.9	12.0	1.60	40	53.5	HAGO
122.5	654.0	11.9	2.40	40	92.7	HAGO
120.3	647.8	11.8	1.60	10	153.6	BETE
121.0	650.7	11.6	2.14	10	263.1	BETE
121.9	648.7	11.8	1.60	20	154.4	BETE
121.4	649.5	11.7	2.12	20	261.9	BETE
120.8	653.9	11.8	1.60	30	155.1	BETE
120.9	653.3	11.8	2.09	30	253.9	BETE
120.8	654.6	11.8	1.58	40	152.3	BETE
119.9	656.0	11.3	2.00	40	232.6	BETE

The PDPA measures intensity of scattered light as a droplet passes through the intersection of two laser beams. The crossing of the two beams forms a fringe pattern and the diameter and velocity of a droplet passing through the fringes can be determined from the time signal of zero crossings [19, 20]. The velocity of the particles can be calculated from the frequency of scattered light, while droplet size is determined from

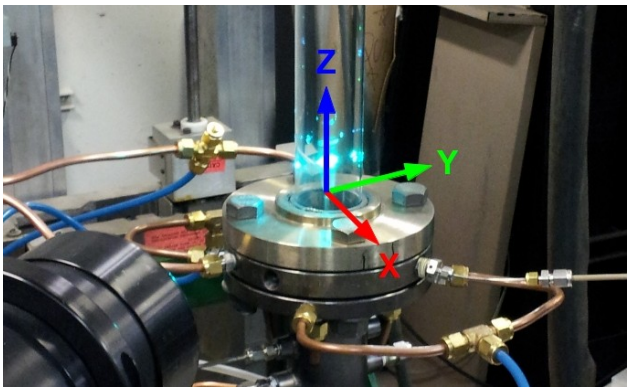

(a) Coordinate system

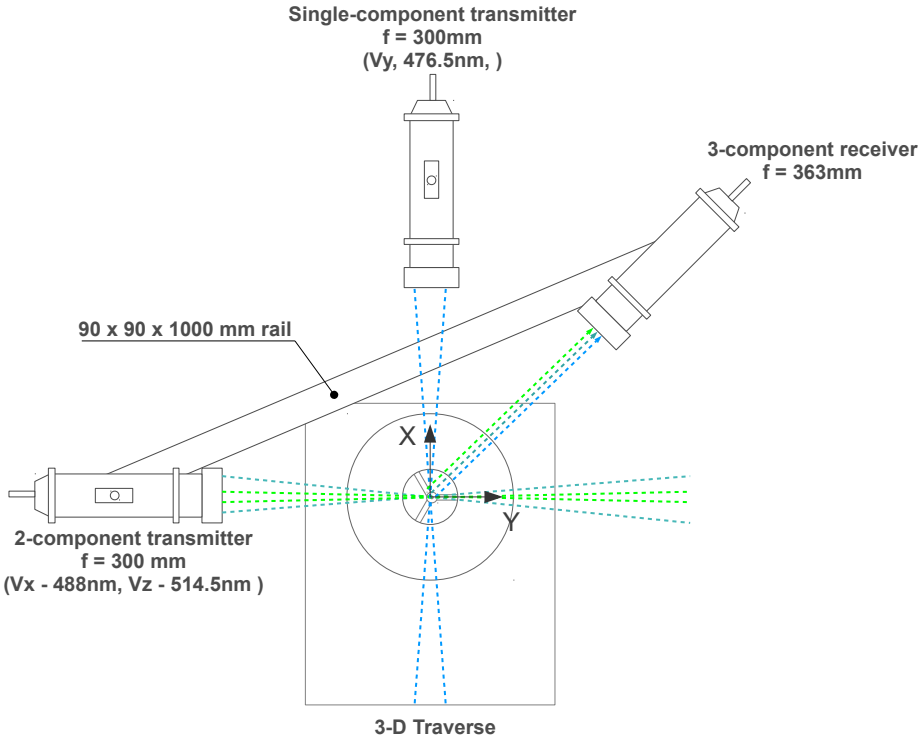

(b) Top view schematic

Figure 4: PDPA setup: (a) Coordinate system on image of HVIF in operation (b) Top-down schematic of PDPA orientation

the phase shift between 2 electrical signals from the scattered light.

Using all droplet measurements at a given location, Arithmetic Mean Diameter (AMD, D_{10}) and Sauter Mean Diameter (SMD, D_{32}) can be calculated using the following equation, where m = 1 and n = 0 for AMD and m = 3 and n = 2 for SMD [21].

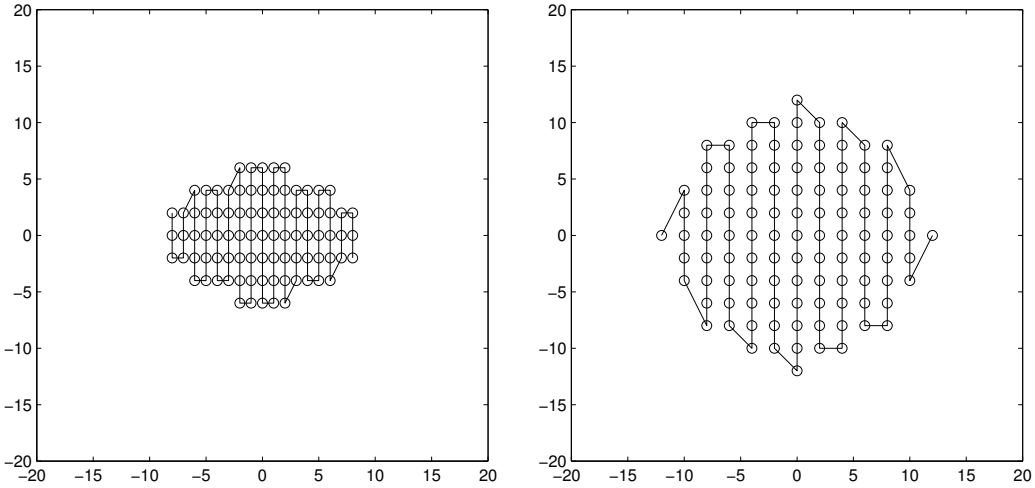

(a) Z = 10mm

(b) Z = 20mm

(c) Z = 30mm

(d) Z = 40mm

Figure 5: Traverse matrices

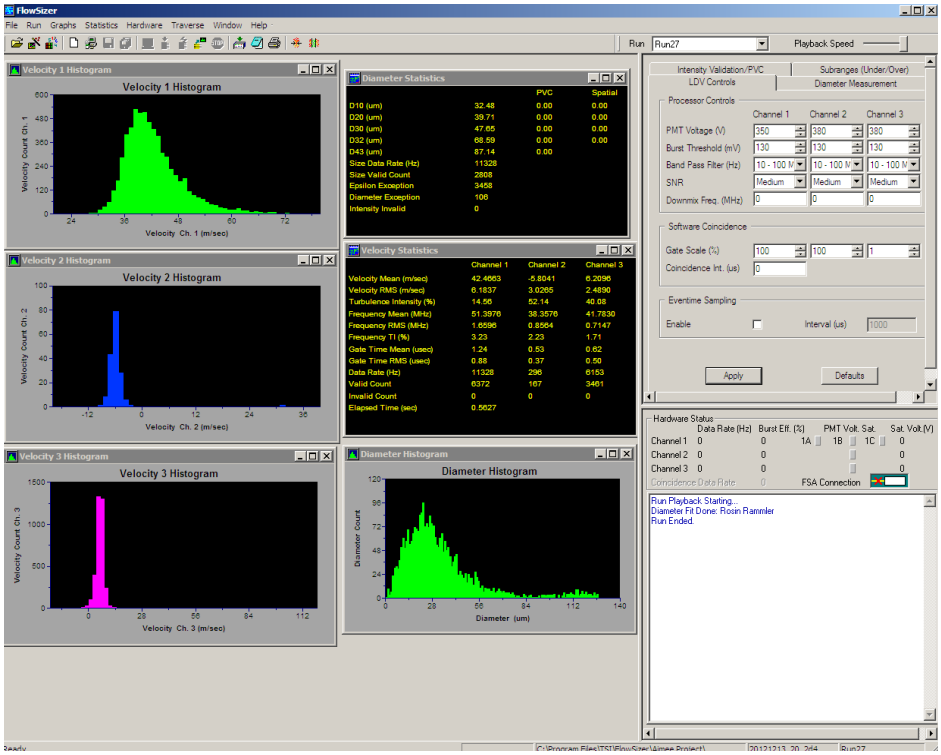

Figure 6: Screenshot of Flowsizer software

$$D_{mn} = \frac{\sum D^m}{\sum D^n}^{\frac{1}{m-n}} \tag{6}$$

The software provided by TSI, called Flowsizer, was used to control the traversing mechanism, collect measurements, and analyze the data to obtain mean velocities, root mean square (RMS) velocities, Arithmetic Mean Diameter (AMD), Sauter Mean Diameter (SMD), and data rate of the droplets. Figure 6 shows a screenshot of the Flowsizer software for one location on the traverse matrix. In this screenshot, all droplets measured are shown in the three velocity histograms on the left (green - axial velocity (V_Z), blue and magenta - components of radial velocity (V_X and V_Y)), and droplet size in the bottom center. From these distributions, both droplet and velocity statistics are calculated and the results are shown in the center column.

Results and Discussion

Nozzle Performance

The spray angle of each of the nozzles at varying flow rates, without co-axial flow, are shown in the pictures in Figure 7. When the flow rate through the HAGO nozzle was varied from 9 g/s to less than 3 g/s, the spray angle varied from 70.2° to 56°. The spray angle of the BETE nozzle changed from 80.2° to 77.3° when the flow rate was halved, from 10 g/s to 5 g/s In these images, both nozzles appear to produce a solid cone spray, but this will be further investigated using PDPA.

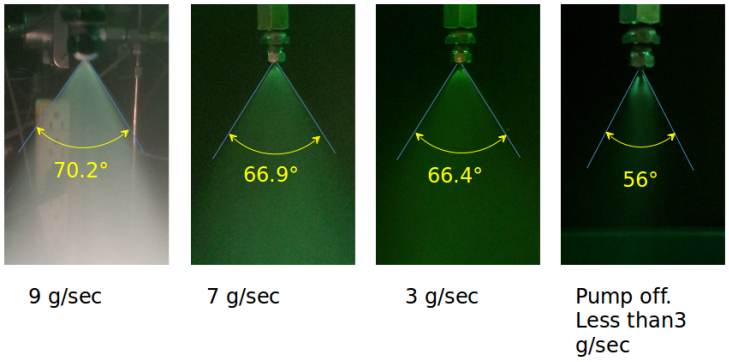

(a) HAGO

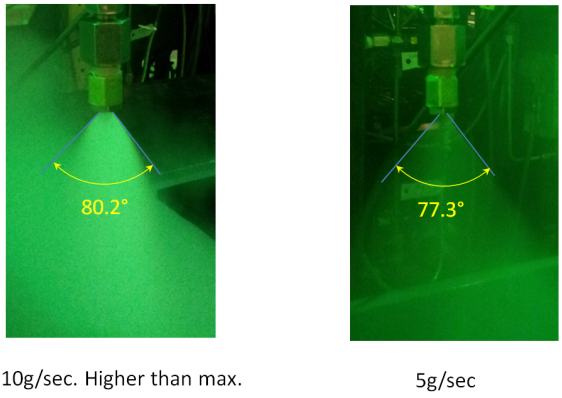

(b) BETE

Figure 7: Spray angle without co-flow of each nozzle

Droplet Distributions

The droplet size distributions for both the HAGO and BETE nozzles are shown in Figure 8. To recreate the histograms displayed using the Flowsizer software, the droplet size bins and droplet count, as were shown in Figure 6, were exported to a comma-separated variables (CSV) file. The bins start at 0.5005 μm and increase by 1.001 μm. Each histogram was recreated from all droplet measurements during a single run, using MATLAB. The histograms shown are from three locations in each cross-section of the spray: the center of the spray (R=0), the edge of the spray (R = R_{max}) and halfway between the center and edge (R = $R_{max}/2$), as shown on the cartoon in Figure 9.

The droplet distributions for the HAGO nozzle in Figure 8a show narrow distributions in the center of the spray that include a small tail due to small numbers of large droplets. As the distance from the center of the spray increases, the droplet distributions widen. As the distance from the nozzle downstream (Z) increases, the total number of droplets decrease and the most frequent droplet size changes from 5.5 μm at 10mm to 10.5 μm at 40mm.

The droplet distributions for the BETE nozzle are shown in Figure 8b. These distributions show that the nozzle produces no droplets in the center of the spray. Where droplets occur, the distributions are narrow and more symmetric than with the HAGO nozzle. The distributions widen closer to the periphery. Note that the entire spray was not captured at the 30mm cross-section and the narrow distribution shown was probably nearer to $R_{max}/2$ than the actual R_{max}.

Comparing the droplet distributions for the two nozzles, the histograms show that the BETE nozzle had much narrower and more symmetric droplet distribution than the HAGO nozzle. Additionally, the most frequent droplet size occurs as a smaller diameter for the BETE nozzle than the HAGO nozzle. While the HAGO nozzle has a somewhat non-uniform droplet distribution, the BETE nozzle is completely lacking in droplets in the center of the flow. This property is detrimental to the goal of achieving a uniform droplet distribution for the future auto-ignition studies.

Droplet Analysis

To further investigate the nozzle performance, droplet counts were analyzed using the Flowsizer software to determine the Arithmetic Mean and Sauter Mean Diameter, and X, Y, and Z axis velocity components. These quantities will be discussed below. The data shown is for the HAGO nozzle at $\dot{m}_{JetA} = 2.40g/s$, V = 123.6m/s, T = 651.4°C, O_2=11.8 % and the BETE nozzle at $\dot{m}_{JetA} = 2.15g/s$, V = 120.8 m/s, T = 652.5°C, O_2=11.7%.

Mean Droplet Size

Arithmetic Mean diameter (AMD) and Sauter Mean diameter (SMD) were calculated at each grid point, in each plane, for all test conditions. From each grid of data, the AMD and SMD along the Y-axis were extracted for each plane and each nozzle at 2.4 g/s for the HAGO nozzle and 2.15 g/s for the BETE nozzle. Note that due to the large pressure drop across the BETE nozzle, 2.15 g/s was the highest achievable flow rate with the current fuel supply system.

Figures 10 and 11 show the AMD and SMD at each grid point along the Y-axis in each plane for both nozzles. The abscissa shows the distance along the Y-axis from the center of the spray normalized by the maximum width of the spray in that plane. For example, at the flow conditions shown, at 40mm, the maximum spray width was 14mm for the HAGO nozzle and 20mm for the BETE nozzle. The average droplet sizes are given in μm.

The two nozzles are advertised as producing a solid cone of droplets. Their design suggests the droplets will have swirl when leaving the nozzle. Due to this, the mean droplet sizes are expected to be fairly uniformly distributed across the spray, with some of the large droplets near the edge due to centrifugal force on the droplets.

The AMD and SMD distributions along the Y-axis were similar for both nozzles. Large droplets are located near the periphery of the spray and the smallest droplets are located in the center. The placement of large droplets is attributed to the nozzle design and the spray having swirl. The HAGO nozzle produced mean droplet sizes of 7-15 μm AMD in the center of the spray and maximum mean droplet sizes of 35 to 50μm near the edge, depending on the distance from the nozzle. The SMD plot for the HAGO nozzle, given in Figure 11a, shows 15 μm SMD in the center and maximum SMD of 70-80 μm near the edge of the spray. These Sauter Mean diameters are as much as twice the Arithmetic Mean diameters. Looking back to Figure

8a, the HAGO histograms show a "tail" in the droplet size distribution. This tail represents a small number of very large droplets in the spray. These large droplets cause larger SMD values due to the D^3 term for calculation of SMD (D_{32}).
The BETE nozzle produces 5 μm AMD droplets in the center of the spray and the average did not change with distance downstream. Due to the wide spray, droplet measurements of the edge of the spray were not captured in all planes, but the maximum droplet size measured ranged from 20 to 50 μm. Calculated SMD for the BETE nozzle was 10 μm in the center and 35 to 70 μm at the edge of the spray. Note that the test section diameter was 45mm. Due to the wide spray angle of the BETE nozzle, at these flow conditions, at approximately 40mm from the nozzle, the spray is as wide as the test section and droplets will be deposited onto the test section walls.
For both nozzles, as the distance from the nozzles increased, the average droplet size increased. As was shown in the histograms, the small droplets have evaporated, and some may have coagulated, to result in larger average values. The BETE nozzle produces smaller droplets than the HAGO nozzle and has a uniform droplet size in the center of the spray, but greater difference in droplet sizes from the center to the edge. SMD does not vary from AMD as much with the BETE nozzles due to more narrow and symmetric droplet distributions, as were shown in Figure 8b. These distributions do not have the long the tail that causes larger SMD then AMD.

AMD and SMD at each point, in each plane (Z = 10, 20, 30, and 40mm), for each flow rate is shown in Appendix A, Figures 16 through 20 and Figures 21 through 25 for both the HAGO and BETE nozzles, respectively.

Velocity

Velocity components were measured in three directions based on the orientation of the PDPA. A schematic of the coordinate system was shown in Figure 4. Droplet velocities in the axial direction (direction of the co-flow / Z-axis) are shown in Figure 12 along the y-axis. As with the droplet diameter plots, the distance from the center of the spray was normalized by the maximum radius of the spray in that plane.

The HAGO nozzle, shown in Figure 12a produces droplet velocities, ranging from 20 to 60 m/s, in the center of the spray where the smallets droplets occured, with maximum velocities of 35 to 65 m/s at approximately $\frac{R}{R_{max}} = 0.3 - 0.4$. The axial velocity of the co-flow was calculated to be about 124 m/s. The maximum velocity achieved with this nozzle, 65 m/s, was 50% of the velocity of the co-flow.

The BETE nozzle produced a less uniform velocity profile than the HAGO nozzle. The center velocities shown range from 15 to 70 m/s while the maximum velocities range from 55 to 95 m/s. For this test, the axial velocity was 120 m/s. This nozzle did produce much faster droplets, with the maximum droplet velocity being 75% of the co-flow velocity. The pressure drop to produce similar flow rates in the BETE nozzle was much greater than with the HAGO nozzle, this could lead to a faster exit velocity.

Droplet velocities in the x-y plane are shown below in Figure 13 for the HAGO nozzle at the same flow conditions as the droplet measurements previously discussed. At 10 mm from the nozzle, there is not a significant component in this plane, as is shown by Figure 13a. As the distance from the nozzle is increased, the swirl in the nozzle provides a radial velocity. The swirl is well illustrated in these figures. The maximum velocity shown in these plots occurs at 20mm from the nozzle, grid point (10, -4). Here the velocity in the X-Y plane is 14.6 m/s. At the same location, the Z-axis velocity is 40.3 m/s. The swirl velocity is 36% of the droplet axial velocity and approximately 12% of the axial velocity of the hot flow.

The droplet velocities with the BETE nozzle are shown in Figure 14. These plots show that near the center of the spray there is some swirl, and near the edge of the spray the velocities are mostly in the radial direction without swirl. Near the very center of the spray, a very small number of droplets were observed so there is more scatter in the data. Additionally, the downstream end of the BETE was more blunt than for the HAGO nozzle and could be causing additional flow disturbances.

Data Rate

Data rate represents the number of droplets per second measured by the PDPA. The data rate along the y-axis in each plane, for both nozzles, is shown in Figure 15 and reported in Hz. For the HAGO nozzle, the data rate is lowest in the center and edges of the spray, where there was a low number of droplets. The low data rate at the edge of the spray shows that the entire spray was captured. In the center of the spray, the data rate ranges from about 1000 to 7000 droplets per second, while the peaks of the data rate range from 10,000 to 45,000 droplets per second. For the BETE nozzle, the area of low droplet frequency is much more exaggerated. No droplets are seen in the center of the spray and the area affected is very large, existing to $\frac{R}{R_{max}} \approx 0.5$. This result reveals that with this nozzle there is a conical area with a radius of half the max radius of the spray where there are no droplets. Data rate for each grid point and all flow conditions is shown in Appendix A, Figures 29 to 33.

Conclusions

- The spray characteristics of two commercial available spray nozzles (HAGO and BETE) were investigated to determine the uniformity of each nozzle with the intention of using the nozzles for future autoignition testing. Both nozzles were advertised as producing a solid-cone spray.
- The nozzles were located in the co-flow of the high velocity ignition facility and embedded in a bullet shaped housing, suported in the center of the test facility by 3 hollow pylons. The test facility operated at 120 m/s, 650°C, 12 $\%O_2$ for all tests. The hollow pylons allowed for cooling of the center body and a 1/16" stainless steel tube supplied fuel and nitrogen purge to the nozzle. A 45mm (1.77") I.D. quartz silica transparent test section allowed for full optical acces
- To characterize the spray, a 3-dimensional phase doppler particle analyzer (PDPA) was used to measure the droplet sizes in 4 planes, Z = 10, 20, 30, and 40 mm from the nozzle. The entire facility was traversed, while the laser system remained stationary. From the droplet measurements, Arithemetic Mean diameter (AMD, D10), Sauter Mean diameter (SMD, D32), velocity, data rate, and histograms were analyzed.
- From the data rate measurements, it was revealed that the BETE nozzle produced a hollow-cone spray. No measureable droplets were observed in the center of the spray. Both nozzles show some non-uniformities in average droplet size from the center to the edge of the spray . Since the nozzles produced swirl, the larger droplets were located near the edge of the spray. By 40mm from the injector, the HAGO nozzle axial velocity distribution was uniform.
- Table 2 shows a summary of the results for each nozzle. Values at center of the spray are compared to the maximum value in the spray. For average diameter and velocity, the maximum value occurred very near to the edge of the spray, while the maximum data rate occured near R/2.

Table 2: Summary of Results for $\dot{m}_{Jet-A}$, Z = 40mm

	HAGO		BETE	
	R = 0	Max	R = 0	Max
AMD (μm)	13	48	6	51
SMD (μm)	17	76	7	64
V_Z (m/s)	60	64	68	86
DR (Hz)	612	10400	0	15500

Flow conditions: HAGO: $\dot{m}_{JetA} = 2.40 g/s$, V = 123.6m/s, T = 651.4°C, O_2=11.8 %
BETE: $\dot{m}_{JetA} = 2.15 g/s$, V = 120.8 m/s, T = 652.5°C, O_2=11.7%

- It is recommended to use the HAGO nozzle for future autoignition testing since it produced the more uniform, solid-cone spray.

Future Work

- Collect CH* chemiluminescence images for an auto-ignition curve for these nozzles and compare to previously obtained data using a jet-in-cross flow
- Perform LDV measurements on the incoming flow to determine its uniformity and turbulence levels
- Develop a larger, 3" diameter facility

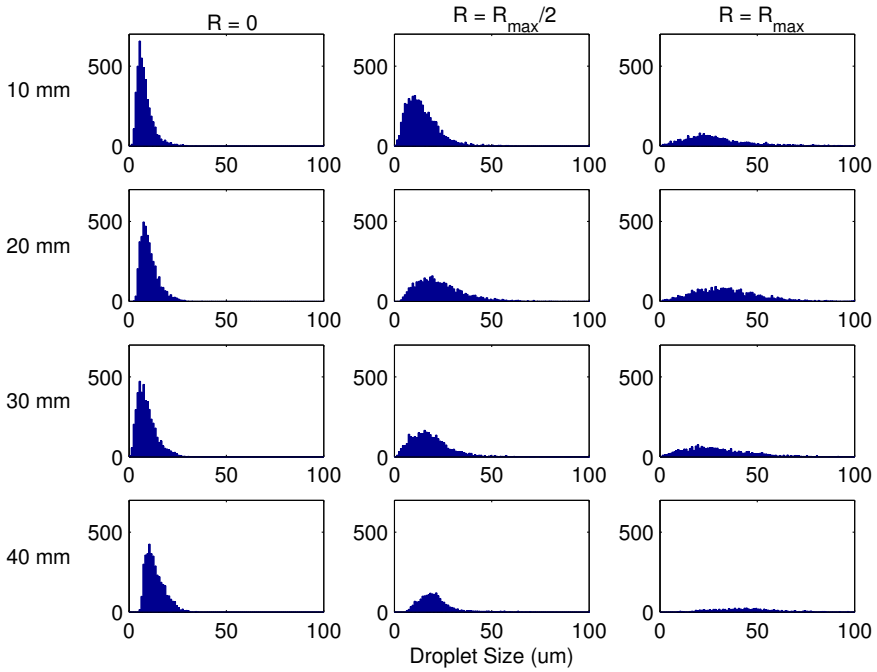

(a) Histograms of droplet sizes at $\dot{m}_{JetA} = 2.40g/s$, V = 123.6m/s, T = 651.4°C, O_2=11.8 %

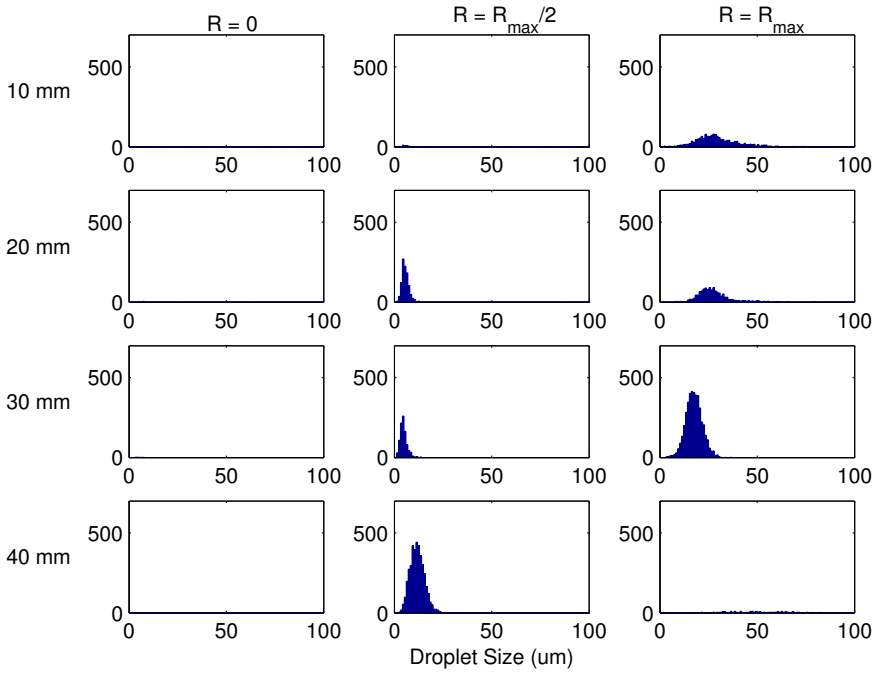

(b) Histograms of BETE droplet sizes at $\dot{m}_{JetA} = 2.15g/s$, V = 120.8 m/s, T = 652.5°C, O_2=11.7%

Figure 8: Histograms at three locations in each cross-section for each nozzle

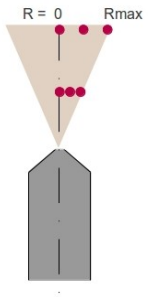

Figure 9: Location in spray of histograms shown in Figure 8

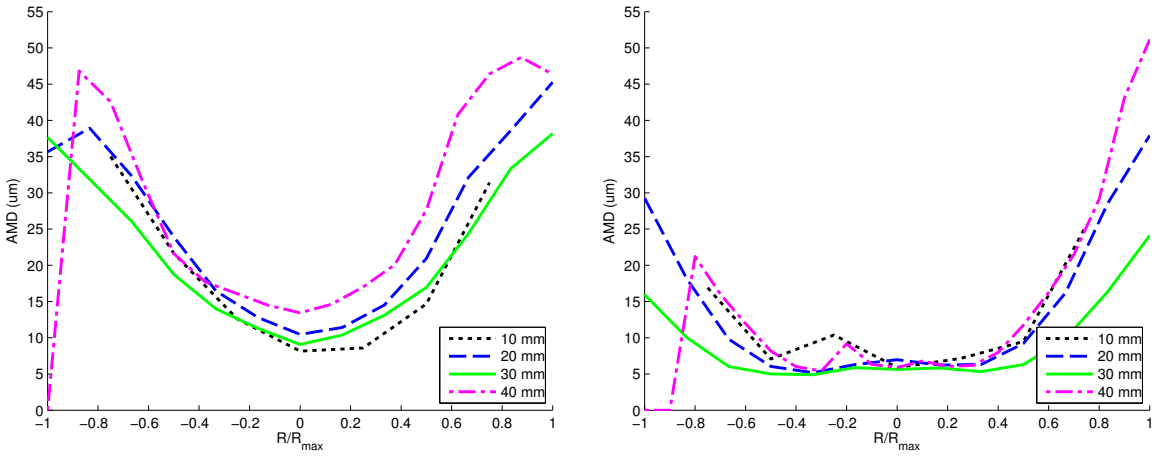

(a) HAGO (b) BETE

Figure 10: AMD (μm) for (a) HAGO: $\dot{m}_{JetA} = 2.40g/s$, V = 123.6m/s, T = 651.4°C, O_2=11.8 % and (b) BETE: $\dot{m}_{JetA} = 2.15g/s$, V = 120.8 m/s, T = 652.5°C, O_2=11.7%

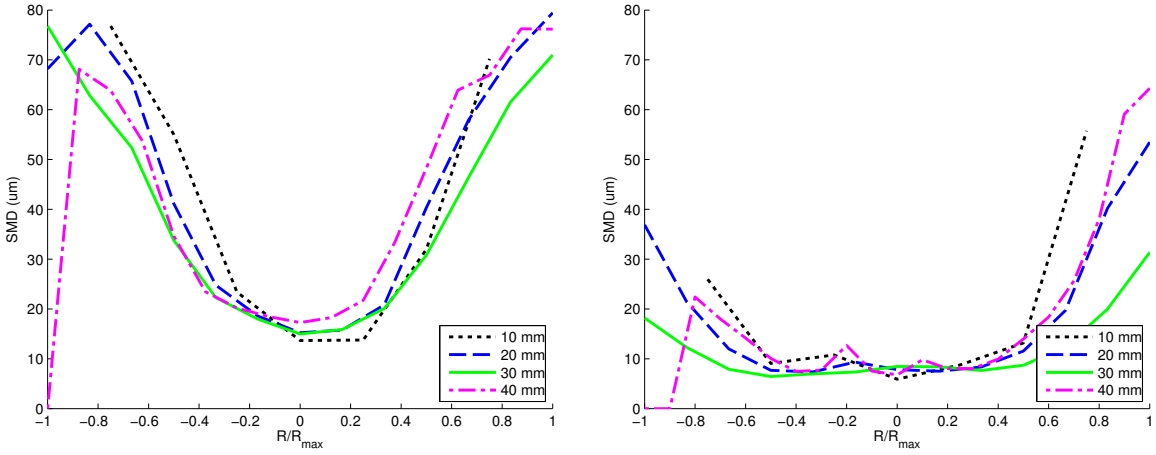

(a) HAGO (b) BETE

Figure 11: SMD (μm) for (a) HAGO: $\dot{m}_{JetA} = 2.40g/s$, V = 123.6m/s, T = 651.4°C, O_2=11.8 % and (b) BETE: $\dot{m}_{JetA} = 2.15g/s$, V = 120.8 m/s, T = 652.5°C, O_2=11.7%

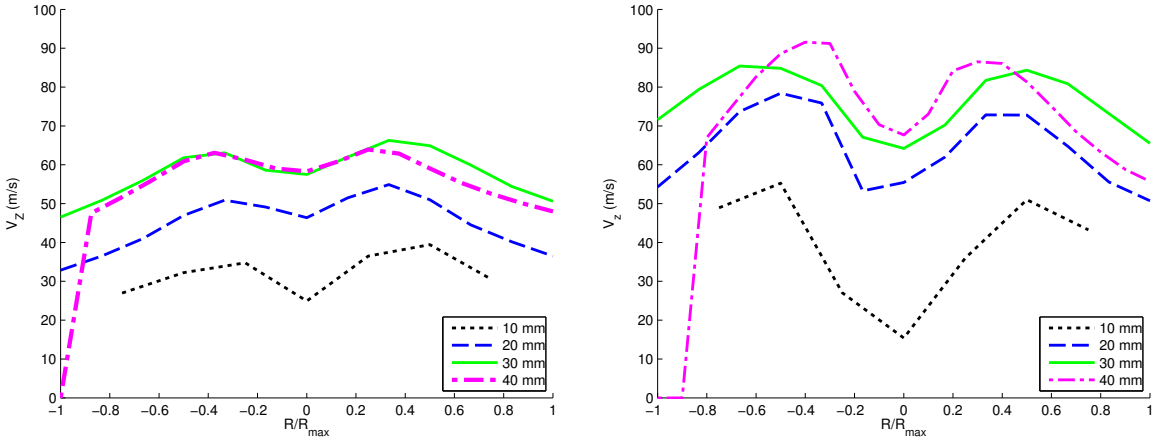

(a) HAGO

(b) BETE

Figure 12: V_Z (m/s) for (a) HAGO: $\dot{m}_{JetA} = 2.40g/s$, V = 123.6m/s, T = 651.4°C, O_2=11.8 % and (b) BETE: $\dot{m}_{JetA} = 2.15g/s$, V = 120.8 m/s, T = 652.5°C, O_2=11.7%

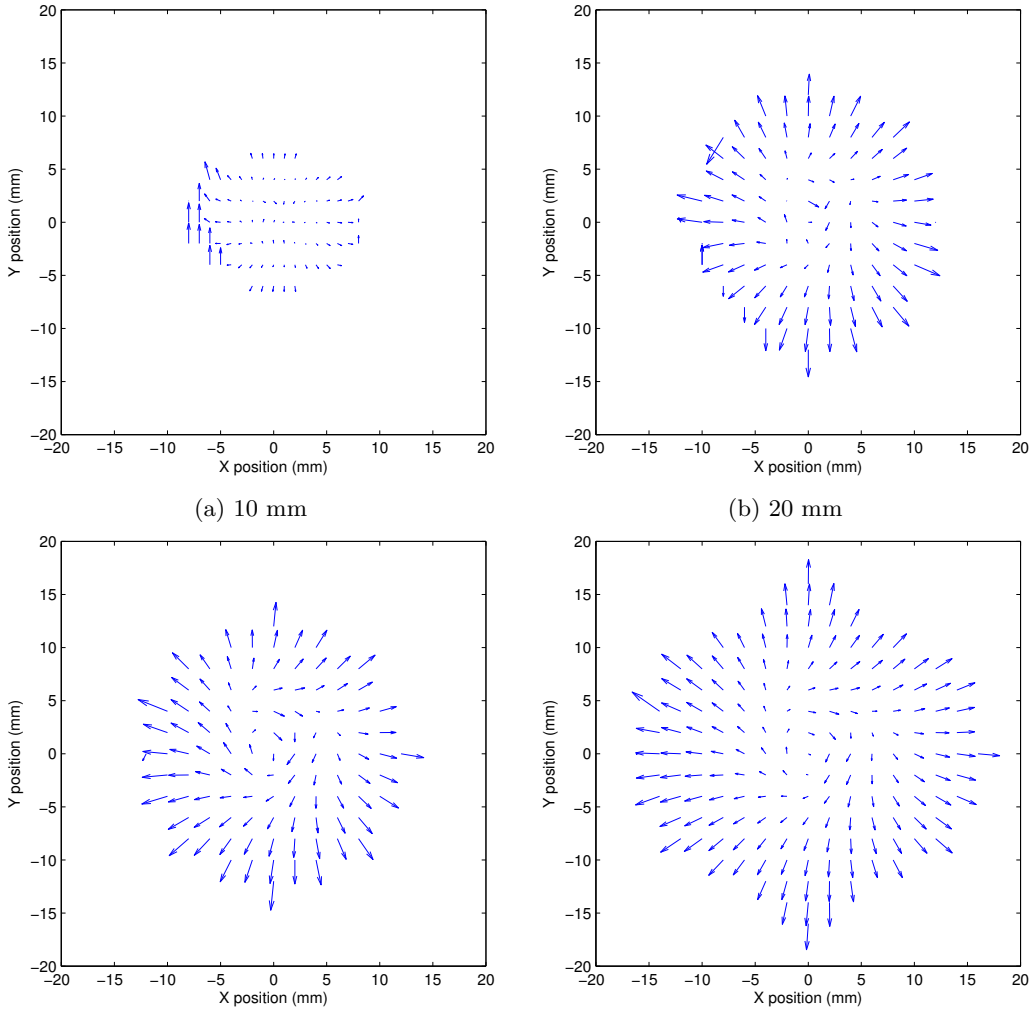

(a) 10 mm

(b) 20 mm

(c) 30 mm

(d) 40 mm

Figure 13: Droplet velocity in the X-Y plane at cross sections 10, 20, 30 and 40 mm from the HAGO spray nozzle at $\dot{m}_{JetA} = 2.40g/s$, V = 123.6 m/s, T = 651.4°C, O_2=11.8%

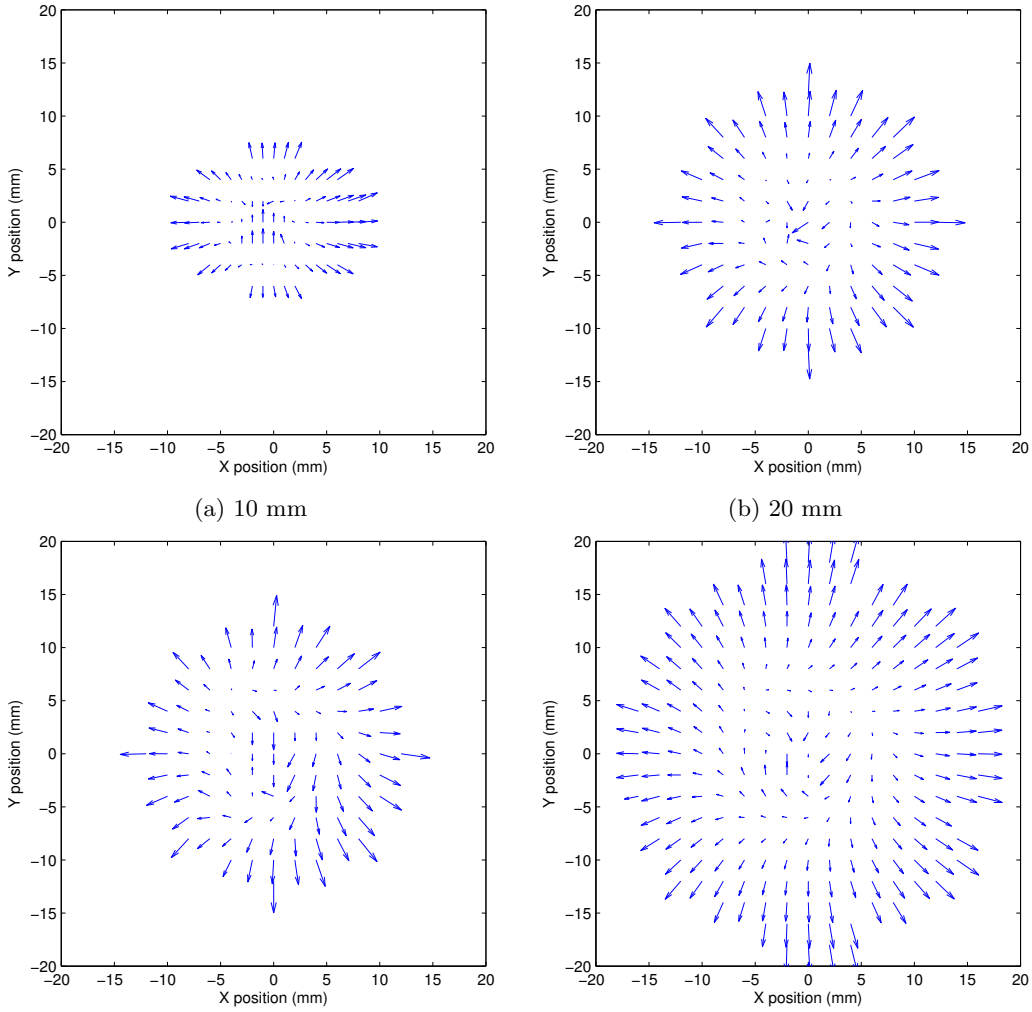

(a) 10 mm

(b) 20 mm

(c) 30 mm

(d) 40 mm

Figure 14: Droplet velocity in the X-Y plane at cross sections 10, 20, 30 and 40 mm from the BETE spray nozzle at $\dot{m}_{JetA} = 2.15g/s$, V = 120.8 m/s, T = 652.5°C, O_2=11.7%

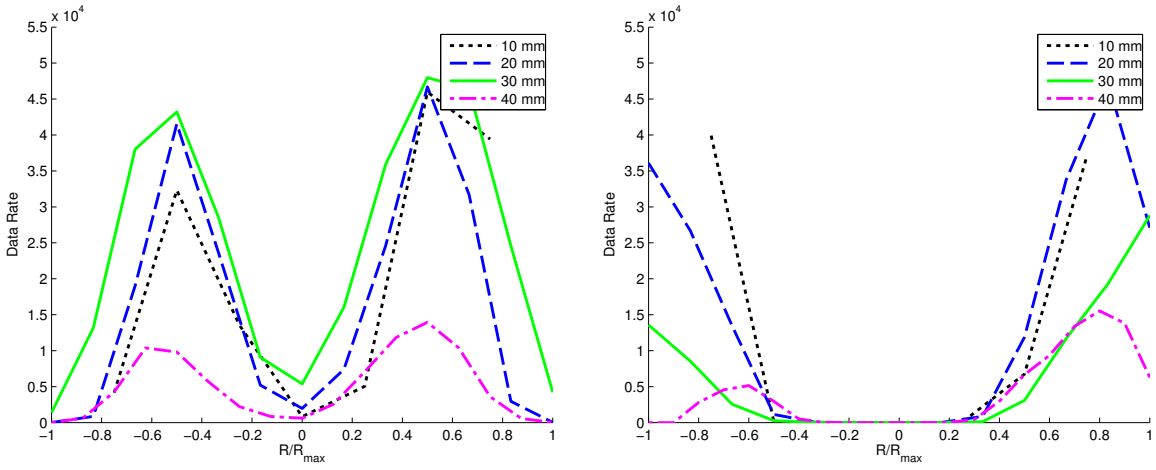

(a) HAGO (b) BETE

Figure 15: Data Rate for (a) HAGO: $\dot{m}_{JetA} = 2.40g/s$, V = 123.6m/s, T = 651.4°C, O_2=11.8 % and (b) BETE: $\dot{m}_{JetA} = 2.15g/s$, V = 120.8 m/s, T = 652.5°C, O_2=11.7%

Bibliography

[1] Williams, Alan Combustion of Liquid Fuel Sprays. Butterworths, London, 1990.

[2] Mullins, B.P. "Studies on the Spontaneous Ignition of Fuels Injected into a Hot Air Stream, Part I-VIII," AGARDograph, No. 4, 1955.

[3] Fleck, J.M. et al., "Autoignition of hydrogen/nitrogen jets in vitiated air crossflows at different pressures," Proc. Combust. Inst., 2012.

[4] Colket, M. B. and Spadaccini, L. J., "Scramjet Fuels Autoignition Study," Journal of Propulsion and Power, Vol. 17, No. 2, March-April 2001.

[5] Marek, C. J., Papthakos, L. C., and Verbulecz, P. W., "Preliminary studies of autoignition and flashback in a premizing-prevaporizing flame tube using Jet-A fuel at lean equivalence ratios," NASA TM X-3526, 1977.

[6] Freeman, G., and Lefebvre, A.H., "Spontaneous Ignition Characteristics of Gaseous Hydrocarbon-Air Mixtures," Combustion and Flame, 58, pp153-162, 1984.

[7] Gokulakrishnan, P., Gaines, G., Klassen, M.S., Roby, R.J., "Autoignition of Aviation Fuels: Experimental and Modeling Study," 43rd AIAA/ASME/ASEE Joint Propulsion Conference, July 2007, Cincinnati, OH, AIAA Paper No.: 2007-5701-138.

[8] Gokulakrishnan, P., Gaines, G., Currano, J., Klassen, M.S., Roby, R.J., "Experimental and Kinetic Modeling of Kerosene-Type Fuels at Gas Turbine Operating Conditions," Journal of Engineering for Gas Turbines and Power, Vol. 139, 2007.

[9] Fuller, C.C., Gokulakrishnan, P., Klassen, M.S., Roby, R.J., and Kiel, B.V., Investigation of the Effects of Vitiated Conditions on the Autoignition of JP-8, 45th AIAA/ASME/ASEE Joint Propulsion Conference, August 2009, Denver, CO, AIAA Paper No.: 2009-4925.

[10] Spadaccini, L.J., and TeVelde, J.A., "Autoignition Characteristics of Aircraft-Type Fuels," NASA CR-159886, June 1980.

[11] Tacina, Robert. Autoignition in a Premixing-Prevaporizing Fuel Duct Using Three Different Fuel Injection Systems at Inlet Air Temperatures to 1250K, NASA TM-82938, May 1983.

[12] Mastorakos, E. and Baritaud, T.A., "Numerical simulations of autoignition in turbulent mixing flows," Combustion and Flame, Vol. 108: 198-223, 1997.

[13] Kruetz. T.G. and Law, C. K, "Ignition in nonpremixed counterflowing hydrogen versus heated air: Computational study with detailed chemistry," Combustion and Flame, Vol. 104: 157-175, 1996.

[14] Dooley, S., Won, S. H., Chaos, M., Heyne, J., Ju, Y., Dryer, F. L., Kumar, K., Sung, C. J., Wang, H., Oehlschlaeger, M. A., Santoro, R. J., and Litzinger, T. A., "A jet fuel surrogate formulated by real fuel properties," Combustion and Flame, Vol. 157, 2003.

[15] Lovett, J.A., Brogan, T.P., Philippona, D.S., Keil, B.V., and Thompson, T.V., "Developmental Needs for Advaced Afterburner Designs," 40th AIAA/ASME/SAE/ASEE Joint Propulsion Conference, July 2004, Fort Lauderdale, FL, AIAA-2004-4192

[16] Cutright, J.T., Neumeier, Y., Zinn, B.T.,, "Ignition Triggering of Afterburner Fuel Using Partial Oxidation Mixtures," Proc. of ASME Turbo Expo, Orlando, FL, June 2009, GT2009-60157.

[17] Birmaher, Shai, "A Method for Aircraft Afterburner Combustion Without Flame Holders," Ph.D. Dissertation, Georgia Institute of Technology, 2009.

[18] Birmaher, S., Zeller, S., Wirfalt, P.W., Neumeier, Y., and Zinn, B.T., "Fuel Injection Scheme for a Compact Afterburner Without Flame Holders," Journal of Engineering for Gas Turbines and Power, V. 130, No. 3, May, 2008.

[19] Bachalo, William D., "Method for measuring the size and velocity of spheres by dual-beam light-scatter interferometry," Applied Optics, Vol. 19 No. 3, 1980.

[20] Bachalo, Williams D., 'Development of the Phase/Doppler Spray Analyzer for Liquid Drop Size and Velocity Characterizations," 20th AIAA/SAE/ASME Joint Propulsion Conference, June 1984, Cincinnati, OH, AIAA-84-1199.

[21] Phase Doppler Particle Analyzer (PDPA)/ Laser Doppler Velocimeter (LDV) Operations Manutal, TSI Incorporated, 2001.

APPENDIX A: Additional Data

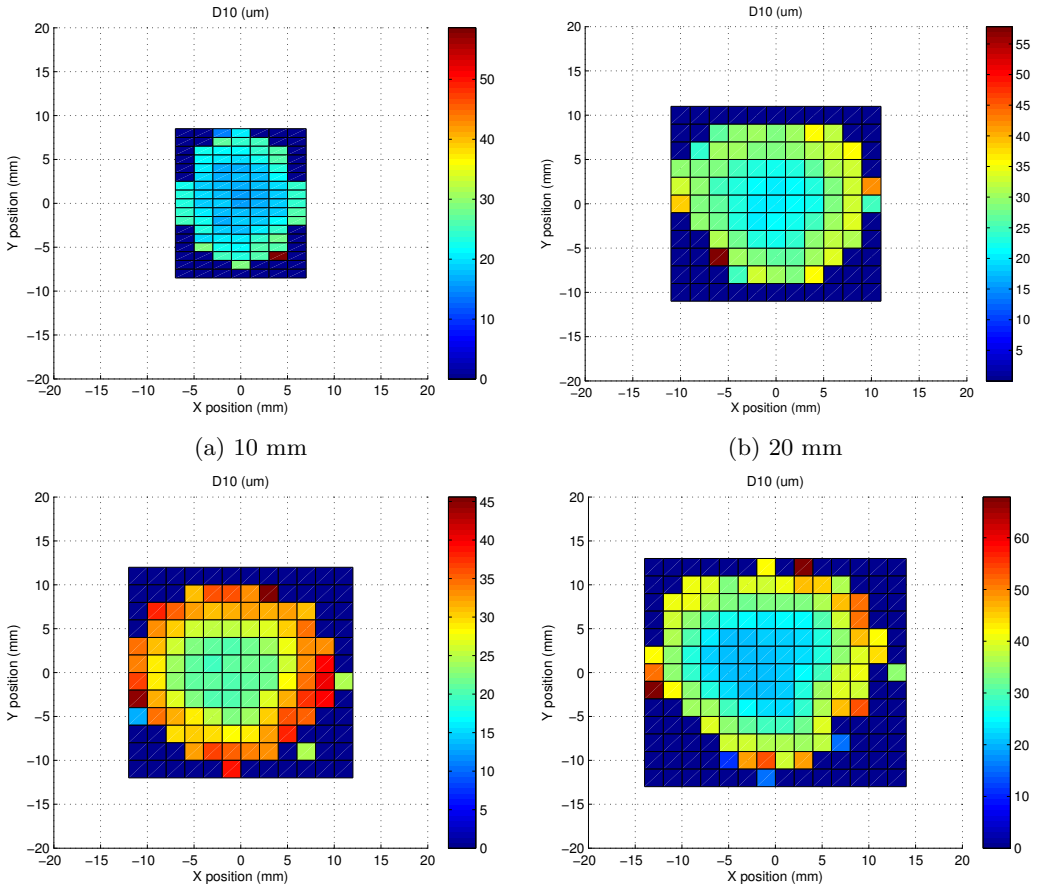

(a) 10 mm

(b) 20 mm

(c) 30 mm

(d) 40 mm

Figure 16: Arithmetic mean diameter at cross sections 10, 20, 30 and 40 mm from the HAGO spray nozzle at $\dot{m}_{JetA} = 0.77g/s$, V = 123.6 m/s, T = 648.6°C, O_2=11.8%

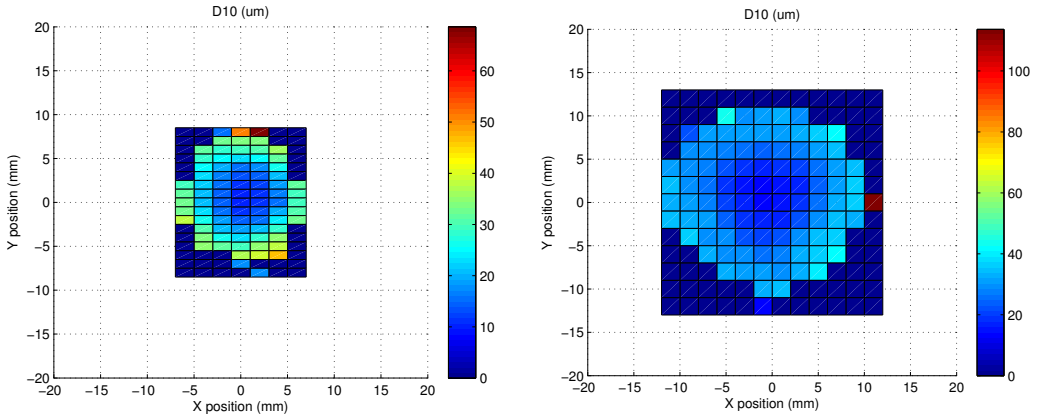

(a) 10 mm

(b) 20 mm

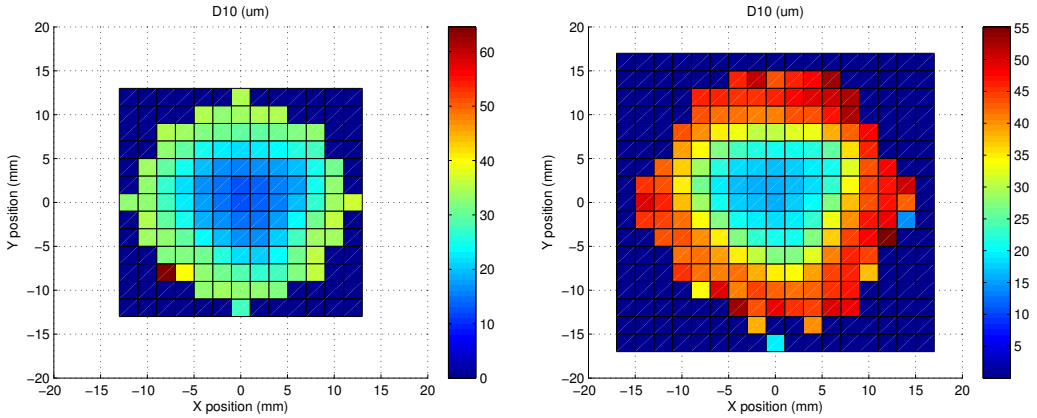

(c) 30 mm

(d) 40 mm

Figure 17: Aritemetic mean diameter at cross sections 10, 20, 30 and 40 mm from the HAGO spray nozzle at $\dot{m}_{JetA} = 1.60g/s$, V = 122.3 m/s, T = 650.7°C, O_2=11.8%

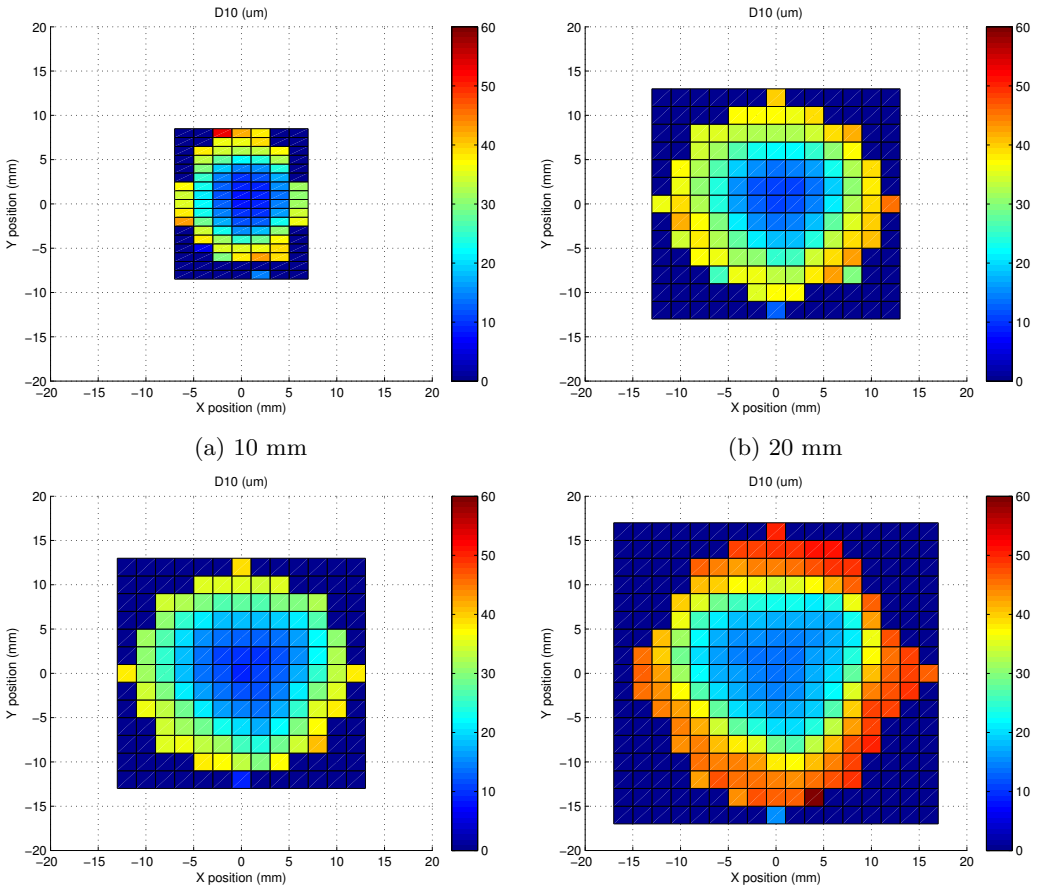

(a) 10 mm

(b) 20 mm

(c) 30 mm

(d) 40 mm

Figure 18: Aritemetic mean diameter at cross sections 10, 20, 30 and 40 mm from the HAGO spray nozzle at $\dot{m}_{JetA} = 2.40g/s$, V = 123.6 m/s, T = 651.4°C, O_2=11.8%

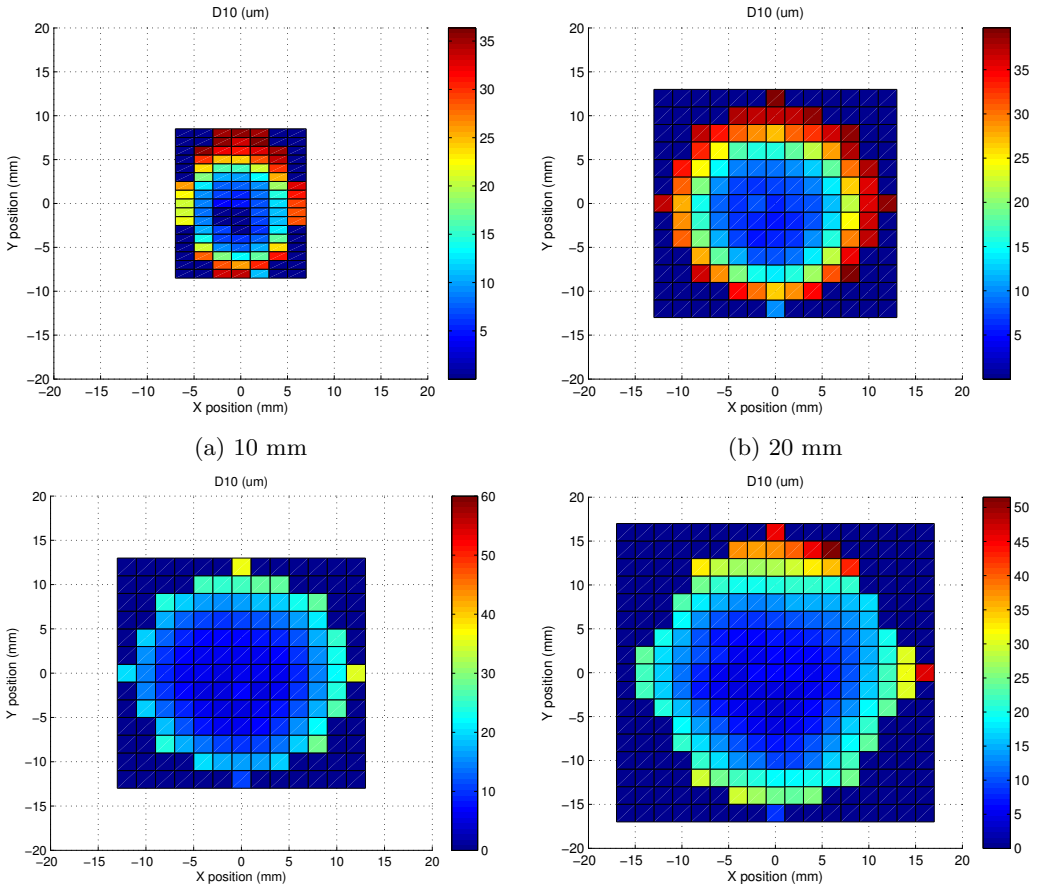

(a) 10 mm

(b) 20 mm

(c) 30 mm

(d) 40 mm

Figure 19: Arithmetic mean diameter at cross sections 10, 20, 30 and 40 mm from the BETE spray nozzle at $\dot{m}_{JetA} = 1.60g/s$, V = 121.0 m/s, T = 651.3°C, O_2=11.8%

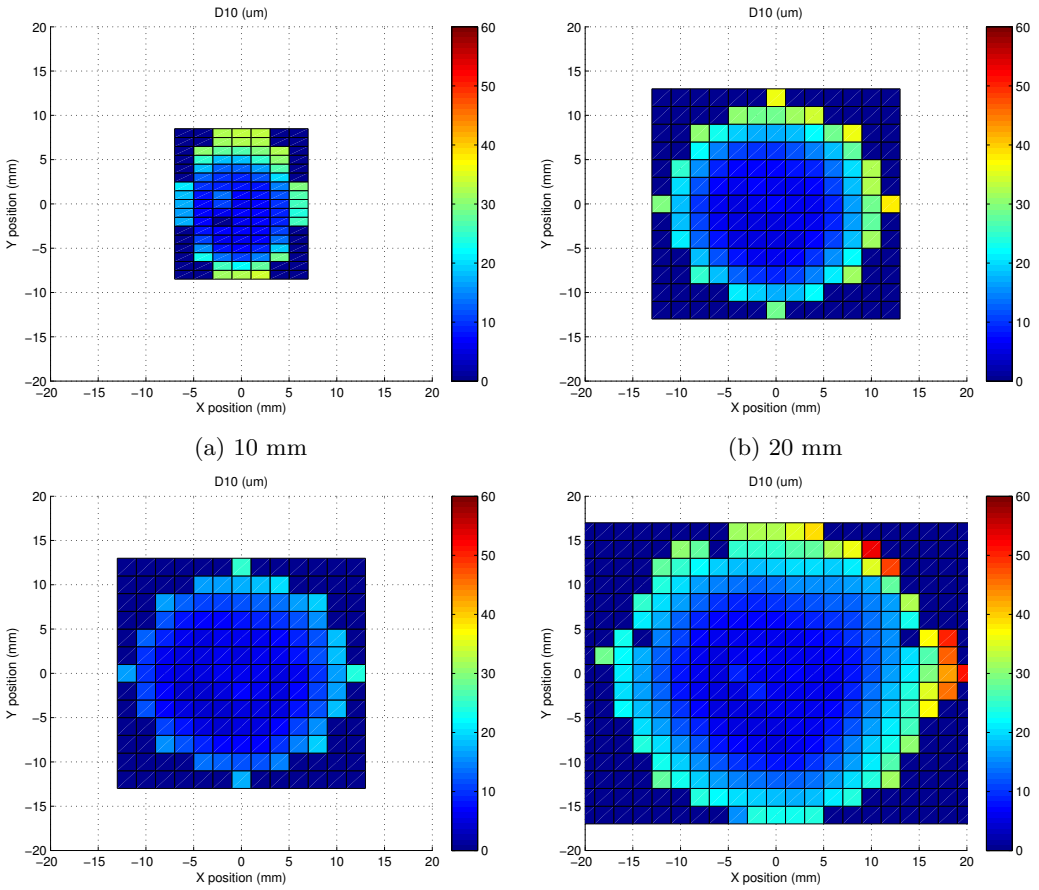

(a) 10 mm

(b) 20 mm

(c) 30 mm

(d) 40 mm

Figure 20: Arithmetic mean diameter at cross sections 10, 20, 30 and 40 mm from the BETE spray nozzle at $\dot{m}_{JetA} = 2.15g/s$, V = 120.8 m/s, T = 652.5°C, O_2=11.7%

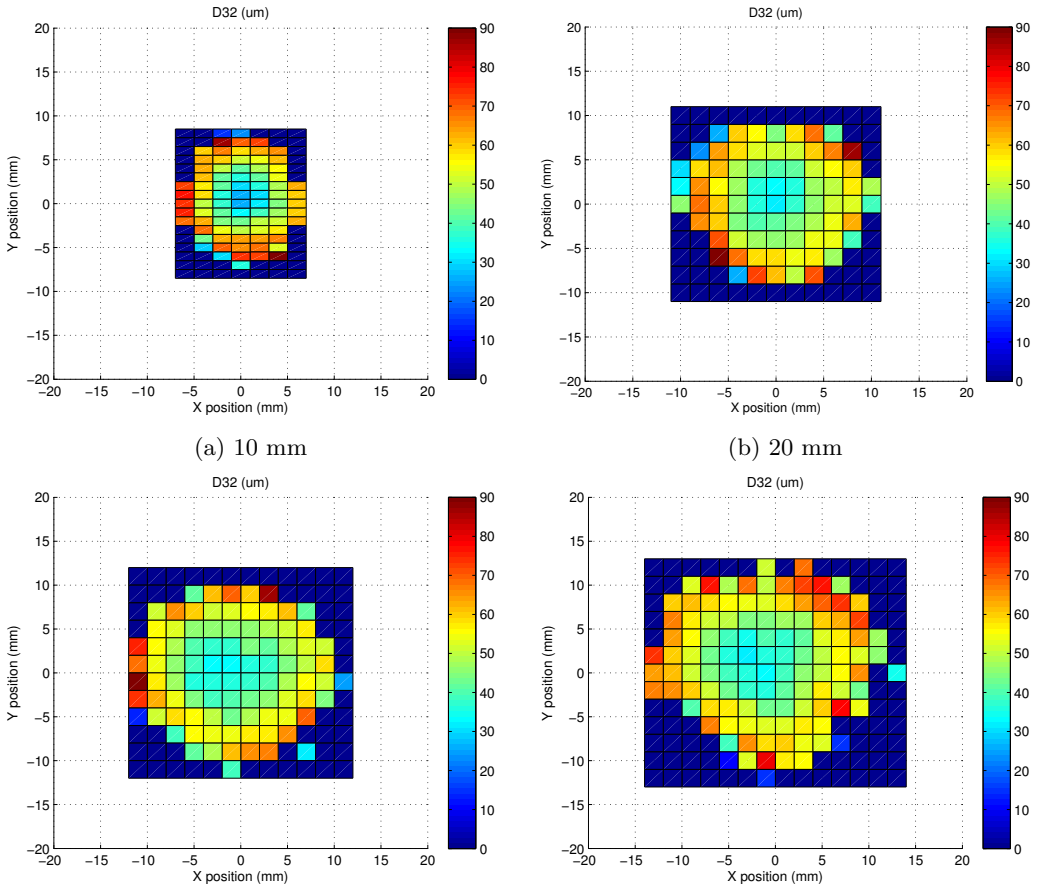

(a) 10 mm

(b) 20 mm

(c) 30 mm

(d) 40 mm

Figure 21: Sauter mean diameter at cross sections 10, 20, 30 and 40 mm from the HAGO spray nozzle at $\dot{m}_{JetA} = 0.77g/s$, V = 123.6 m/s, T = 648.6°C, O_2=11.8%

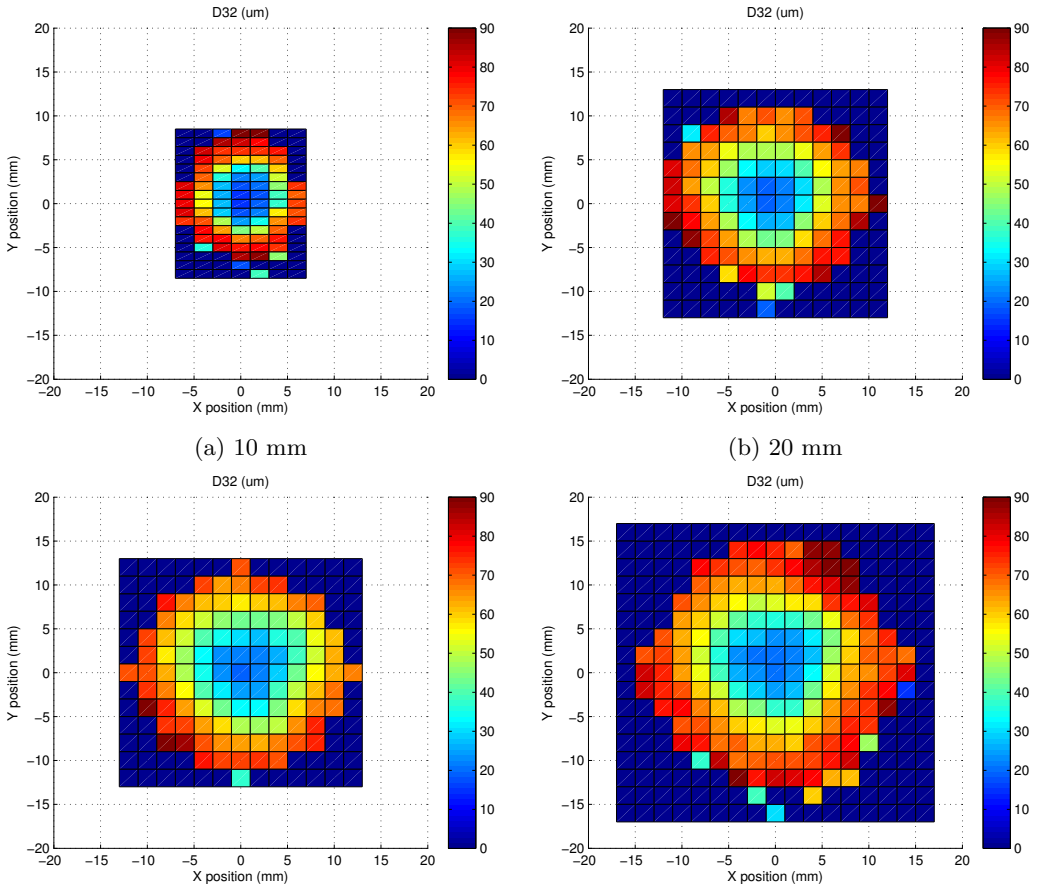

(a) 10 mm

(b) 20 mm

(c) 30 mm

(d) 40 mm

Figure 22: Sauter mean diameter at cross sections 10, 20, 30 and 40 mm from the HAGO spray nozzle at $\dot{m}_{JetA} = 1.60g/s$, V = 122.3 m/s, T = 650.7°C, O_2=11.8%

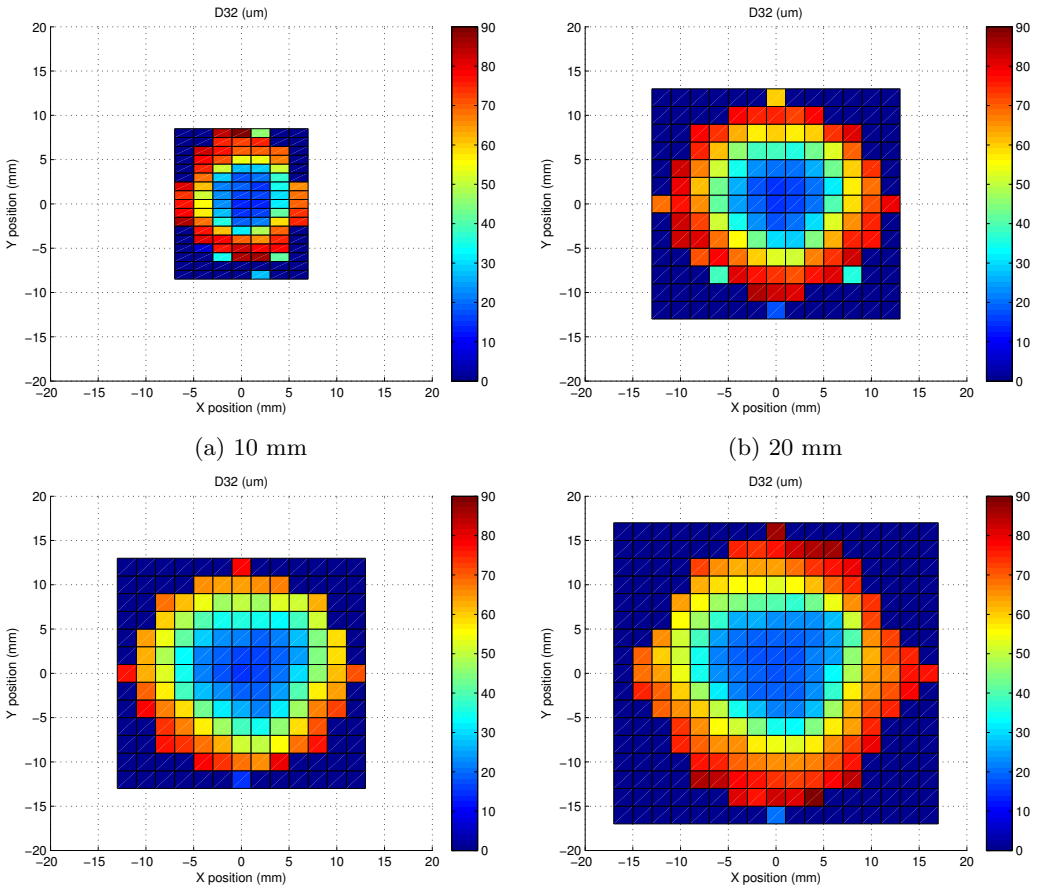

(a) 10 mm

(b) 20 mm

(c) 30 mm

(d) 40 mm

Figure 23: Sauter mean diameter at cross sections 10, 20, 30 and 40 mm from the HAGO spray nozzle at $\dot{m}_{JetA} = 2.40g/s$, V = 123.6 m/s, T = 651.4°C, O_2=11.8%

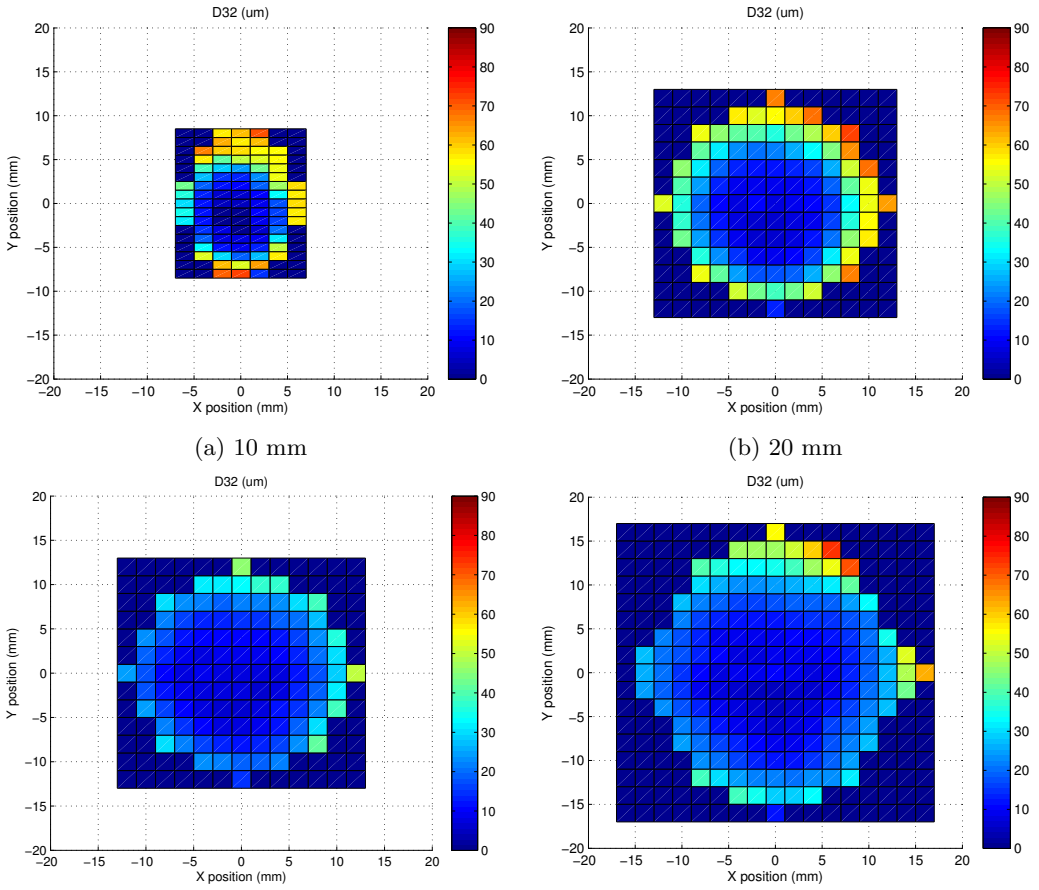

(a) 10 mm

(b) 20 mm

(c) 30 mm

(d) 40 mm

Figure 24: Sauter mean diameter at cross sections 10, 20, 30 and 40 mm from the BETE spray nozzle at $\dot{m}_{JetA} = 1.60g/s$, V = 121.0 m/s, T = 651.3°C, O_2=11.8%

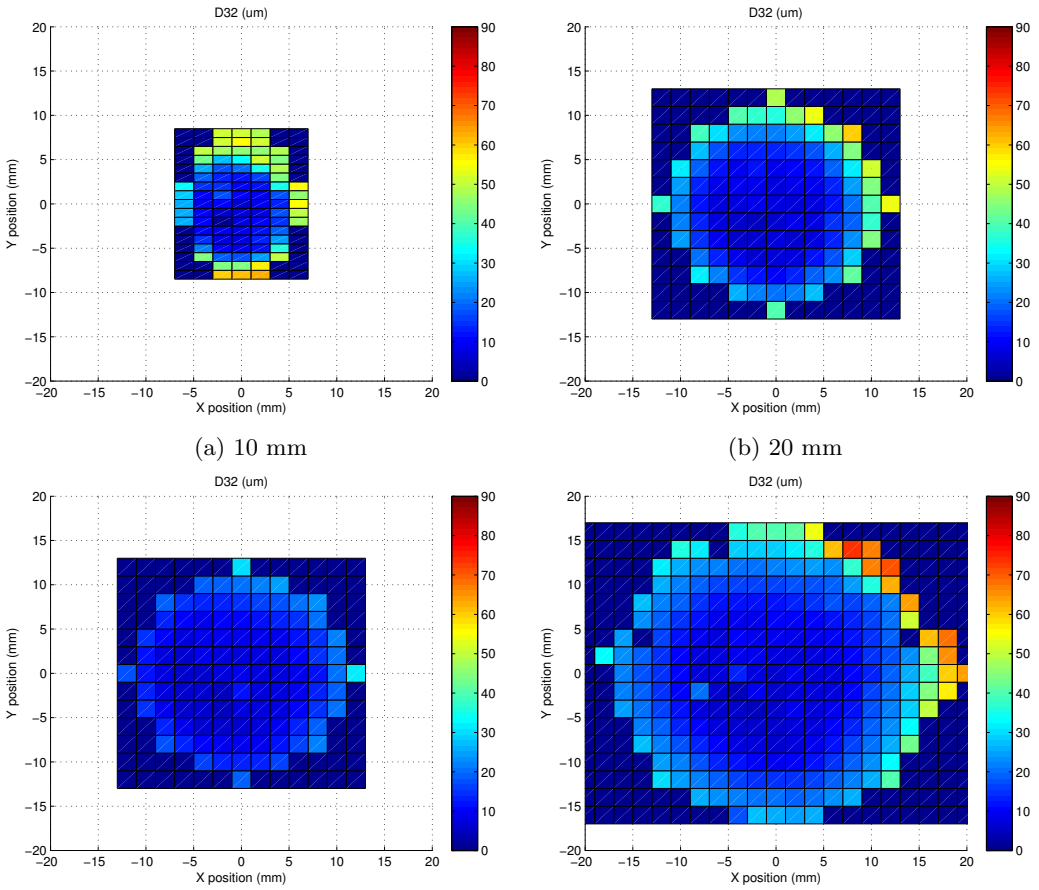

(a) 10 mm

(b) 20 mm

(c) 30 mm

(d) 40 mm

Figure 25: Sauter mean diameter at cross sections 10, 20, 30 and 40 mm from the BETE spray nozzle at $\dot{m}_{JetA} = 2.15g/s$, V = 120.8 m/s, T = 652.5°C, O_2=11.7%

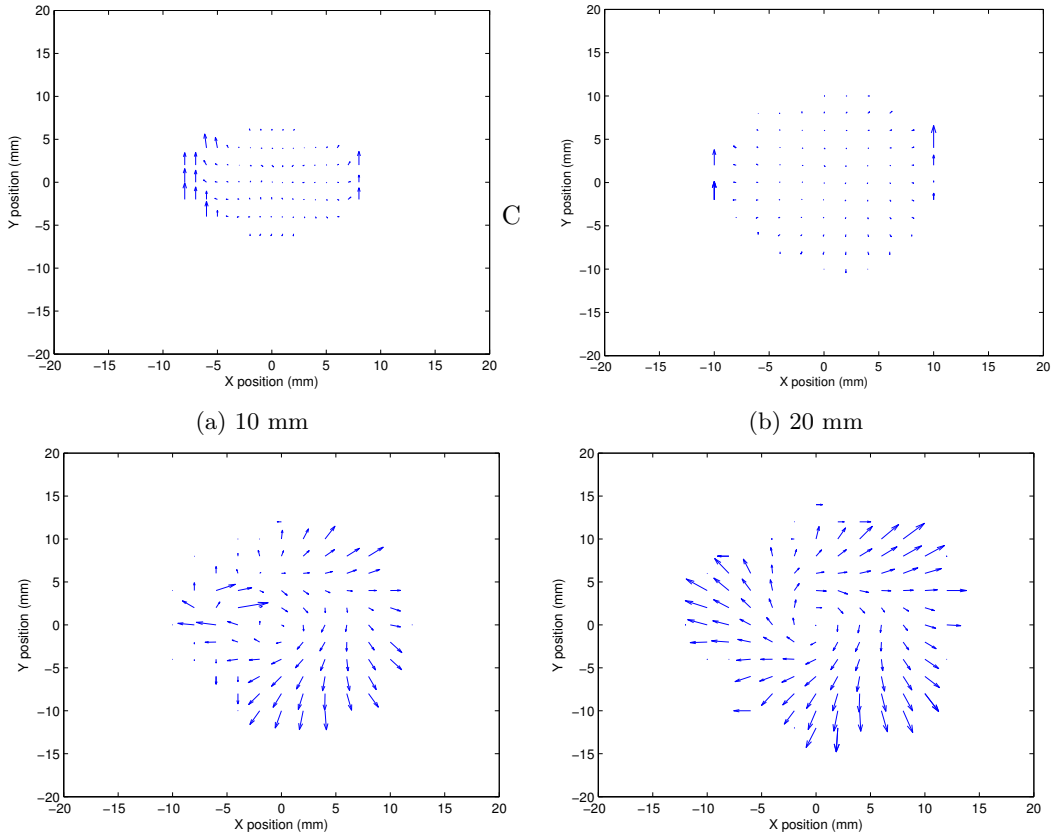

(a) 10 mm

(b) 20 mm

(c) 30 mm

(d) 40 mm

Figure 26: Velocity in the X-Y plane at cross sections 10, 20, 30 and 40 mm from the HAGO spray nozzle at $\dot{m}_{JetA} = 0.77g/s$, V = 123.6 m/s, T = 648.6°C, O_2=11.8%

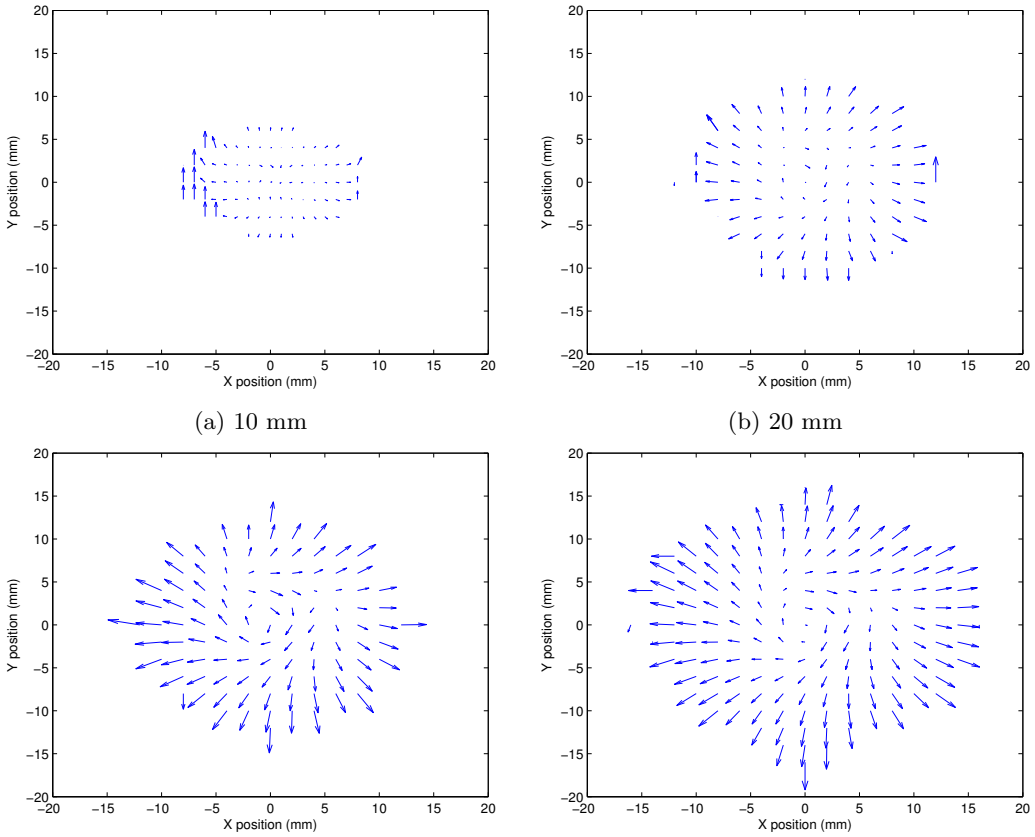

(a) 10 mm

(b) 20 mm

(c) 30 mm

(d) 40 mm

Figure 27: Velocity in the X-Y plane at cross sections 10, 20, 30 and 40 mm from the HAGO spray nozzle at $\dot{m}_{JetA} = 1.60g/s$, V = 122.3 m/s, T = 650.7°C, O_2=11.8%

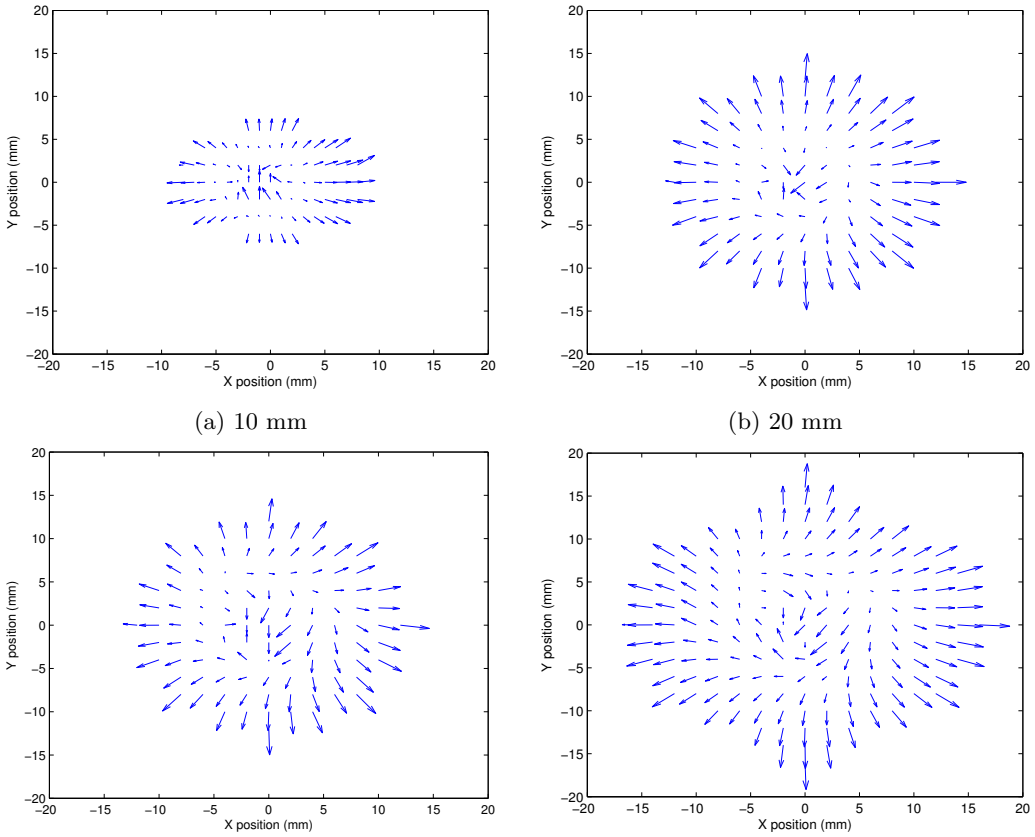

(a) 10 mm

(b) 20 mm

(c) 30 mm

(d) 40 mm

Figure 28: Velocity in the X-Y plane at cross sections 10, 20, 30 and 40 mm from the BETE spray nozzle at $\dot{m}_{JetA} = 1.60g/s$, V = 121.0 m/s, T = 651.3°C, O_2=11.8%

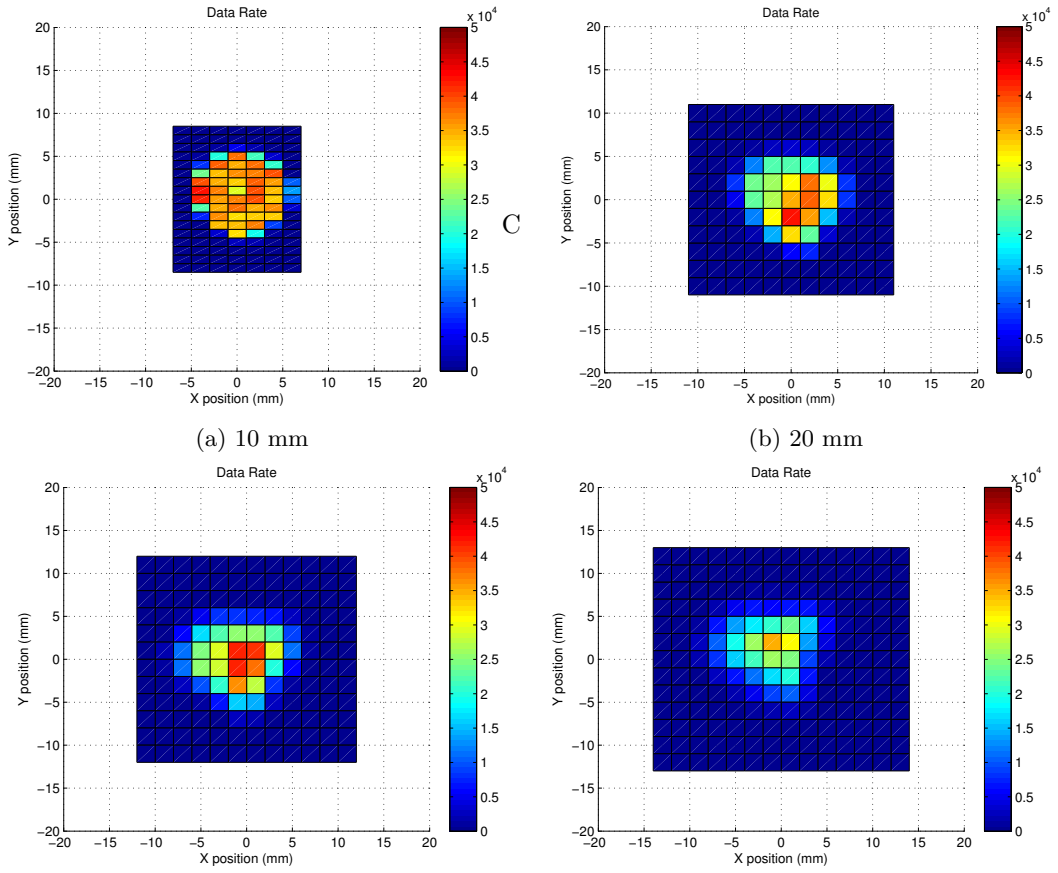

(a) 10 mm

(b) 20 mm

(c) 30 mm

(d) 40 mm

Figure 29: Data rate at cross sections 10, 20, 30 and 40 mm from the HAGO spray nozzle at $\dot{m}_{JetA} = 0.77g/s$, V = 123.6 m/s, T = 648.6°C, O_2=11.8%

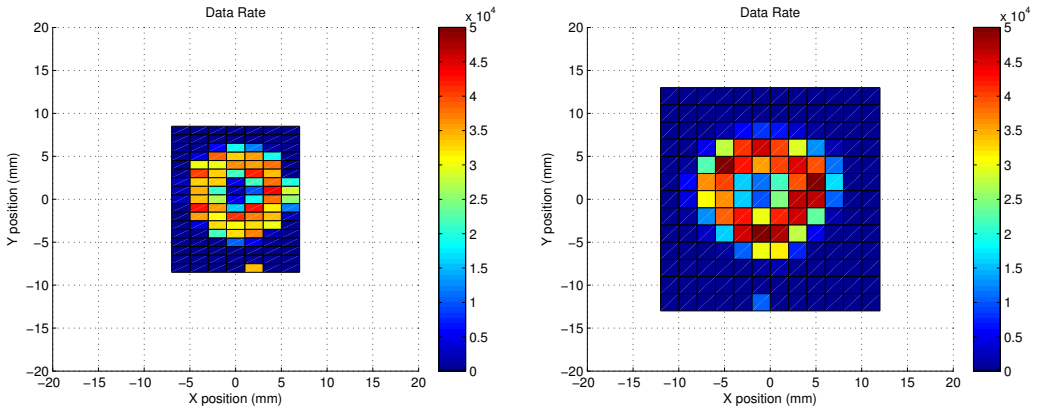

(a) 10 mm

(b) 20 mm

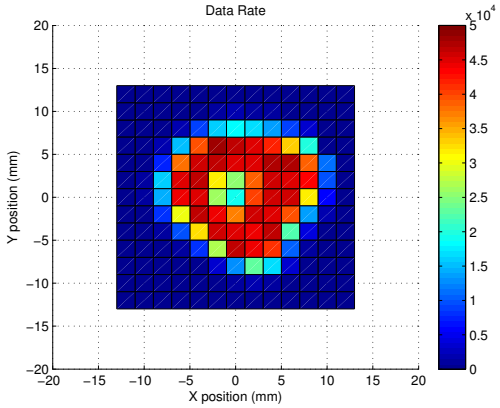

(c) 30 mm

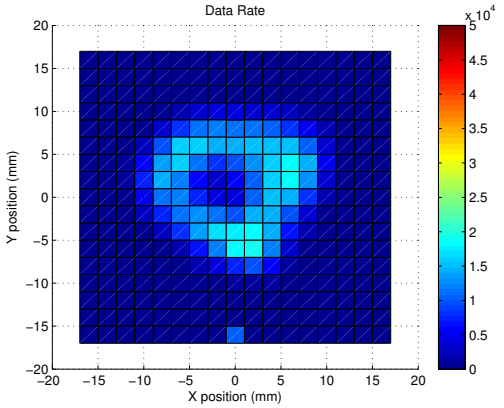

(d) 40 mm

Figure 30: Data rate at cross sections 10, 20, 30 and 40 mm from the HAGO spray nozzle at $\dot{m}_{JetA} = 1.60 g/s$, V = 122.3 m/s, T = 650.7°C, O_2=11.8%

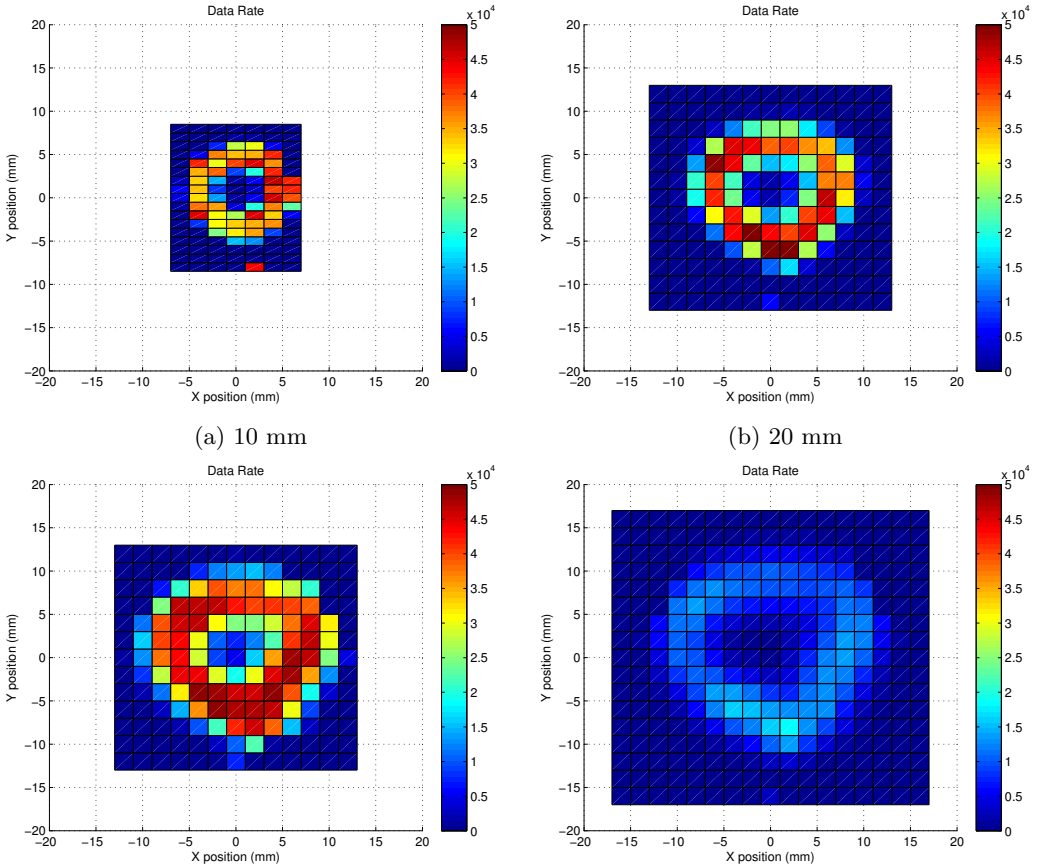

(a) 10 mm

(b) 20 mm

(c) 30 mm

(d) 40 mm

Figure 31: Data rate at cross sections 10, 20, 30 and 40 mm from the HAGO spray nozzle at $\dot{m}_{JetA} = 2.40 g/s$, V = 123.6 m/s, T = 651.4°C, O_2=11.8%

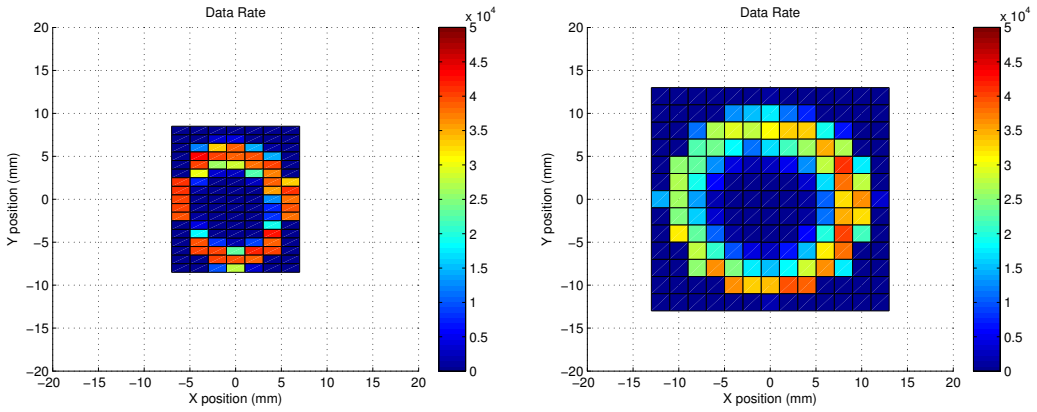

(a) 10 mm

(b) 20 mm

(c) 30 mm

(d) 40 mm

Figure 32: Data Rate at cross sections 10, 20, 30 and 40 mm from the BETE spray nozzle at $\dot{m}_{JetA} = 1.60g/s$, V = 121.0 m/s, T = 651.3°C, O_2=11.8%

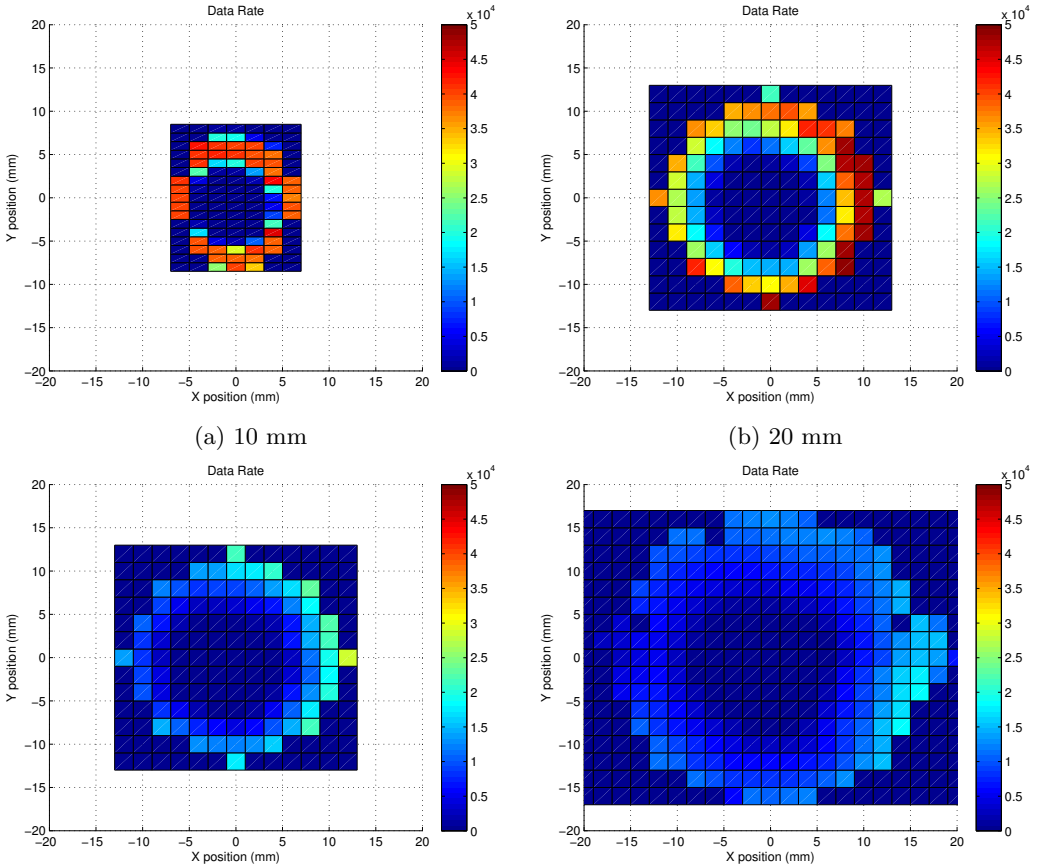

(a) 10 mm

(b) 20 mm

(c) 30 mm

(d) 40 mm

Figure 33: Data rate at cross sections 10, 20, 30 and 40 mm from the BETE spray nozzle at $\dot{m}_{JetA} = 2.15g/s$, V = 120.8 m/s, T = 652.5°C, O_2=11.8%

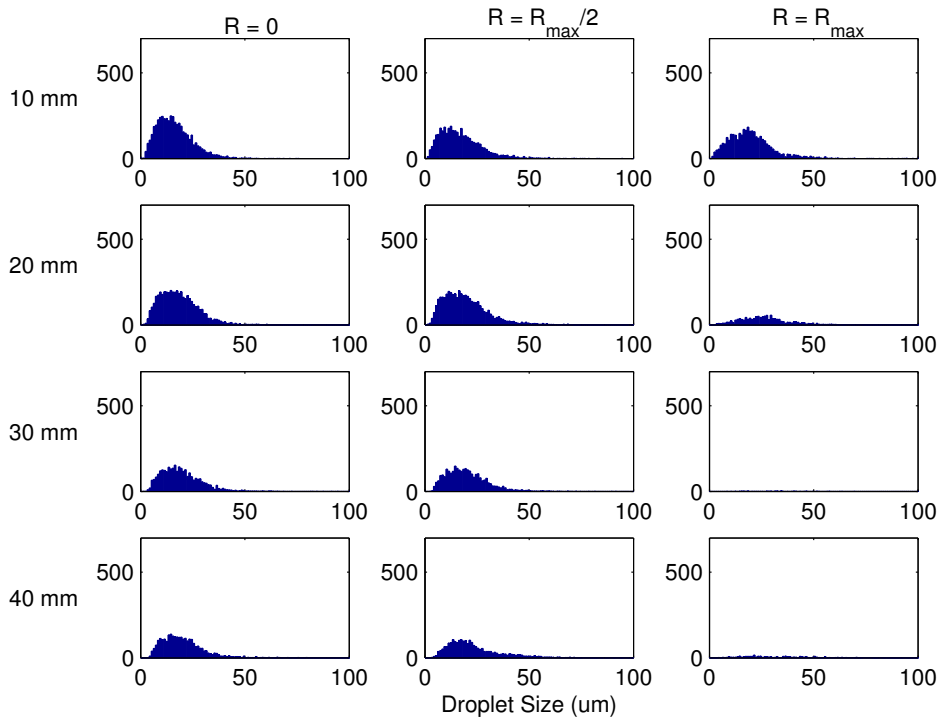

Figure 34: Histograms of droplet size for HAGO spray nozzle at $\dot{m}_{JetA} = 0.77g/s$, V = 123.6 m/s, T = 648.6°C, O_2=11.8%

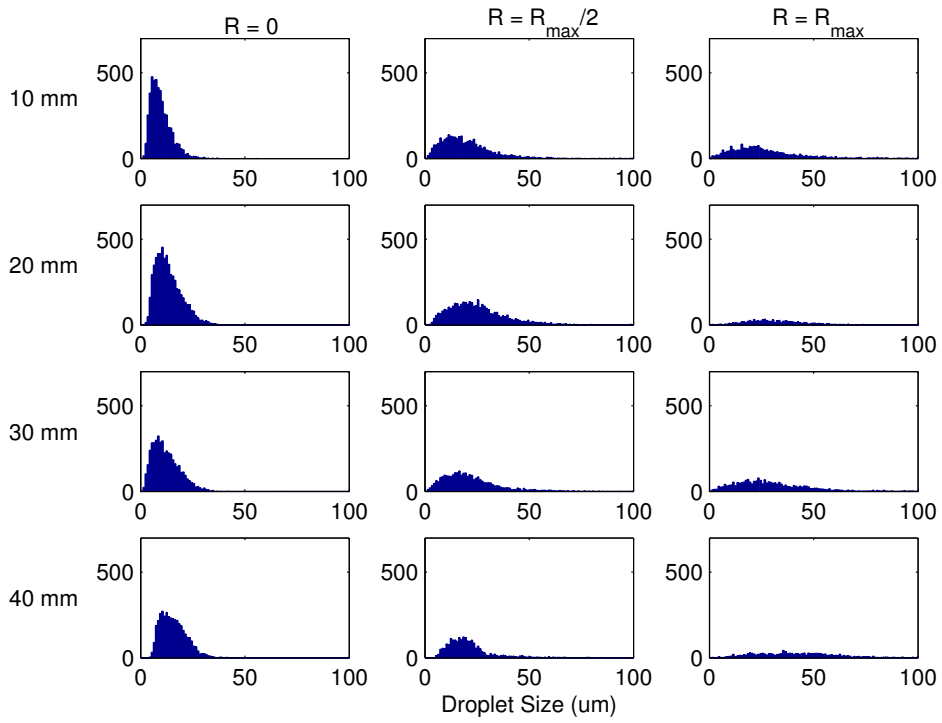

Figure 35: Histograms of droplet size for the HAGO spray nozzle at $\dot{m}_{JetA} = 1.60g/s$, V = 122.3 m/s, T = 650.7°C, O_2=11.8%

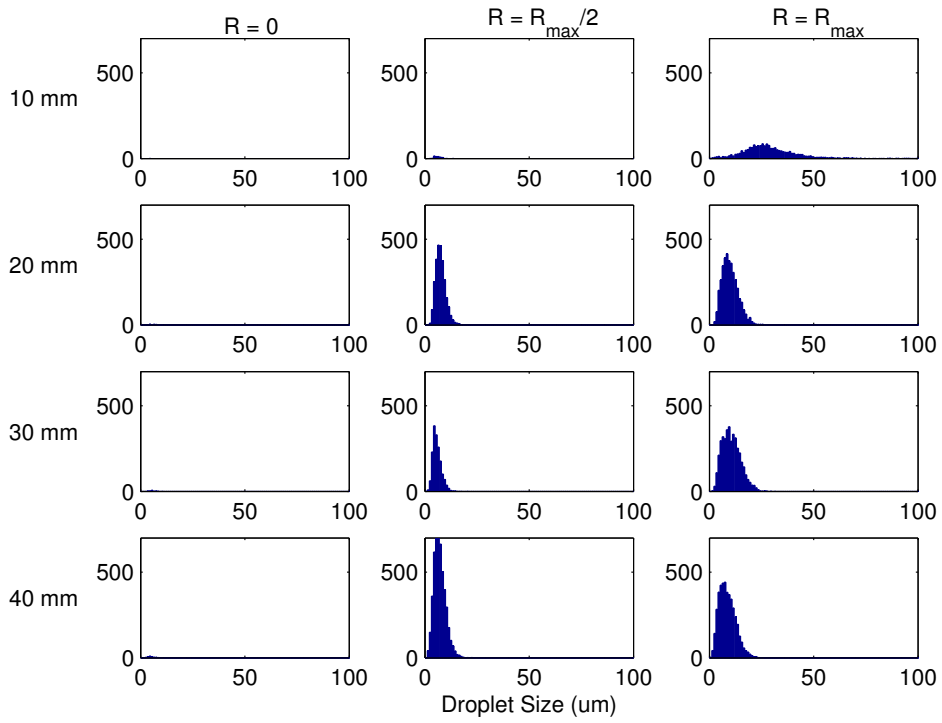

Figure 36: Histograms for droplet size for the BETE spray nozzle at $\dot{m}_{JetA} = 1.60g/s$, V = 121.0 m/s, T = 651.3°C, O_2=11.8%